Energy supply per neuron is constrained by capillary density in the mouse brain

Abbreviated title: Supply-limited energy use per neuron in the brain

Lissa Ventura-Antunes[1,2] and Suzana Herculano-Houzel[2,3,4*]

[1]Instituto de Ciências Biomédicas, Federal University of Rio de Janeiro, RJ, Brazil.

[2]Department of Psychology, Vanderbilt University, Nashville, TN, USA.

[3]Department of Biological Sciences, Vanderbilt University, Nashville, TN, USA.

[4]Vanderbilt Brain Institute, Vanderbilt University, Nashville, TN, USA.

*Corresponding authors: suzana.herculano@vanderbilt.edu , lissa.ventura.antunes@vanderbilt.edu

Manuscript contains 31 pages, 9 figures, no extended figures, 6 Tables.

Numbers of words: 231 in Abstract, 647 in Introduction, 1305 in Discussion.

Conflict of interest: The authors declare no competing interests.

Acknowledgments: Thanks to Louise Botelho, Felipe Tenório and Marina Ricardo for contributing to image analysis, and to Prof. Doug Rothman for insightful discussions. This work was supported by a Scholar Award from the James S. McDonnell Foundation and Vanderbilt start-up funds to SHH, and by a CAPES fellowship to LVA. SHH conceived the study, LVA executed all data acquisition, and both authors analyzed data and wrote the manuscript.

Abstract

Neuronal densities vary enormously across sites within a brain. Does the density of the capillary bed accompany the presumably larger energy requirement of sites with more neurons, or with larger neurons, or is energy supply constrained by a mostly homogeneous capillary bed? Here we find evidence for the latter across various sites in the mouse brain and show that as a result, the ratio of capillary cells per neuron, and thus presumably blood and energy supply per neuron, decreases uniformly with increasing neuronal density and therefore smaller average neuronal size across sites. Additionally, we find that local capillary density is also not correlated with local synapse densities, although there is a small but significant correlation between lower neuronal density (and therefore larger neuronal size) and more synapses per neuron within the restricted range of 6,500-9,500 across cortical sites. Further, local variations in the glial/neuron ratio are also not correlated with local variations in number of synapses per neuron or local synaptic densities. These findings suggest that it is not that larger neurons, neurons with more synapses, or even sites with more synapses *demand* more energy, but simply that larger (and thus fewer) neurons have more energy available per cell, and to its synapses as a whole, than smaller (and thus more numerous) neurons due to competition for limited resources supplied by a capillary bed of fairly homogeneous density throughout the brain.

Significance Statement

The brain is an expensive organ and at rest already uses nearly as much energy as during sensory activation. To ultimately determine whether the high energy cost of the brain is driven by an unusually high energy demand by neurons or constrained by capillary density in the organ, we examine whether sites in the mouse brain with more neurons, larger neurons, or more synapses

have more capillary supply, and find instead that capillary density is mostly homogeneous across brain structures. We propose that neurons are constrained to using what energy is available, with little evidence for adjustments according to local demand, which explains its high risk of ischemia and vulnerability to states of compromised metabolism, including normal aging.

Introduction

The human brain ranks second amongst organs in absolute energy cost at rest only to the liver (Rolfe and Brown, 1997; Mink et al., 1981; Aschoff et al., 1971). Such high cost is commonly attributed to synaptic-mediated neuronal activity (Attwell and Laughlin, 2001; Harris et al., 2012; Ames, 2000), and is entirely met by molecules supplied from the blood and provided to neurons through glial cells whose metabolism is coupled to neuronal activity (Magistretti, 2006; Pellerin and Magistretti, 2016). The high energy cost of the brain, liver and heart puts them at high risk of damage by conditions such as aging that compromise metabolism and oxygen supply (Leach et al., 1998). Elucidating what determines the high energetic cost of the brain is central to understanding healthy and abnormal brain function.

Brain bioenergetics researchers typically consider that the high energetic cost of the brain is driven by a steep energetic *requirement* of neurons, due to costs related to synaptic activity and membrane repolarization (Attwell and Laughlin, 2001; Howarth et al., 2010; Harris et al., 2012). However, energetic use can be determined by *demand* only if it is matched dynamically by a non-limiting supply; otherwise, it is constrained by energetic *supply* that limits work. The former is the case of modern cities where electricity supplied to homes is non-limiting, and demand is free to vary, but is always met; the latter is the case in rural homes that already consume most of what little electricity they are supplied, and cannot sustain both an electric shower and air conditioning running simultaneously (Banavar et al., 2002). In biology, this is evident in hummingbirds, forced into torpor when food is insufficient (Hainsworth et al., 1977).

How much the elevated rate of energy use by the brain represents of its energetic supply is a key open question. Importantly, there is reason to suspect that brain energy use at rest is already close to the limits established by supply. First, both local glucose use and blood flow at

rest depend linearly on local capillary density in rat (Klein et al., 1986) and monkey (Noda et al., 2002). Task-related variations in local cerebral blood flow (CBF) are very small, in the order of 2%, and of at most 8% in primary sensory areas, such that total CBF remains remarkably constant throughout the day of healthy individuals (Schölvinck et al., 2008; Lin et al., 2010). These small local variations in CBF happen with hardly any capillary recruitment (Kuschinsky and Paulson, 1992; Hudetz, 1997). Additionally, blood flow rates in the resting brain are already as high as first achieved in skeletal muscle during exercise (Madsen et al., 1993; Jie et al., 2014).

Here we examine whether the distribution of capillaries in the brain is consistent with a supply-limiting or a demand-based scenario. To that end, we determine whether capillary density is homogeneous throughout the mouse brain regardless of local variations in local neuronal density, which would be expected if it were determined in a system-wide manner by physical scaling limitations (Banavar et al., 2002); or whether it varies coordinately with local neuronal densities, which would be consistent with demand-based reorganization of the capillary bed in response to use, whether because sites with more neurons have higher energy use simply because of the larger number of neurons, or because larger neurons (in sites of lower local neuronal densities) require more energy individually (Attwell and Laughlin, 2001). To gain insight on the particular issue of energy availability per neuron, we calculate its proxy, the local endothelial-to-neuronal-cell (E/N) ratio, and examine how it varies locally in the mouse brain depending on local neuronal densities. Finally, we examine whether variations in energy availability per neuron might also be related to local variations in numbers of synapses per neuron, by combining our data with direct counts of synapse densities in identified locations in the mouse brain published recently (Zhu et al., 2018).

Material and Methods

Ethics Statement: All animal use in this project was approved by the Committee on Ethical Animal Use of the Health Sciences Center (CEUA-CCS), Federal University of Rio de Janeiro (UFRJ) with protocol number 01200.001568/2013-87.

Experimental design: We used structured illumination confocal imaging to allow quantification of cells and microvasculature in individual sections (2D) and stacks (3D) of multiple locations in the brain of five adult mice. In two of those mice, subjected to detailed 3D quantification, brain microvasculature was revealed by injection of a fluorescent tracer (FITC-Dextran, see below) into the caudal vein; in the other three, subjected to much more time-efficient 2D quantification, brain capillaries were revealed by immunohistochemistry against collagen IV, which labels the basal lamina of blood vessels, once we established that measurements of capillary density were indistinguishable between the two labeling methods (see below). Immunohistochemistry against the neuronal marker NeuN (Mullen et al., 1992) was used to reveal neurons; glial cells were identified by exclusion of neurons and capillary-associated cells from the total number of cell nuclei visualized with DAPI.

We quantified capillary area fraction (which is identical to capillary volume fraction) and cell densities in ten easily definable brain structures (cerebral cortical gray and white matter, cerebellar gray and white matter, thalamus, hypothalamus, striatum, hippocampal and cerebellar granular and molecular layers) imaged with structured confocal illumination in a total of 5 mice, comprising 867 stacks analyzed in 3D (two mice, total of 32,270 cells) and 750 ROI acquired and analyzed in 2D (three mice, total of 196,206 cells; Table 1). While image stacks allow detailed visualization of microvasculature in 3D, two-dimensional analysis of image montages

allows for larger sites with larger cell populations to be sampled in less time (Fig. 1). We thus compared the two approaches in this study to determine whether 2D analysis of the distribution of capillaries and neurons are a viable and more efficient alternative to 3D quantification.

Structure	Mouse 01	Mouse 02	Mouse 03	Mouse 04	Mouse 05
CerCx, GM	32 stacks 2,516 cells	54 stacks 3,495 cells	76 ROI 63,022 cells	57 ROI 17,613 cells	34 ROI 12,053 cells
CerCx, WM	60 stacks 1,497 cells	69 stacks 2,531 cells	59 ROI 2,651 cells	19 ROI 1,636 cells	27 ROI 3,931 cells
Thalamus	83 stacks 4,349 cells	42 stacks 1,997 cells	21 ROI 9,096 cells	15 ROI 5,442 cells	16 ROI 3,634 cells
Hypothalamus	45 stacks 2,816 cells	34 stacks 1,861 cells	13 ROI 5,358 cells	12 ROI 2,260 cells	11 ROI 2,125 cells
Striatum	59 stacks 3,283 cells	43 stacks 2,693 cells	29 ROI 15,539 cells	16 ROI 6,284 cells	18 ROI 6,467 cells
Hippocampus, ML	40 stacks 137 cells	73 stacks 202 cells	9 ROI 136 cells	9 ROI 88 cells	8 ROI 118 cells
Hippocampus, GL	25 stacks 470 cells	21 stacks 368 cells	13 ROI 726 cells	13 ROI 310 cells	9 ROI 609 cells
Cerebellum, GL	37 stacks 2,105 cells	23 stacks 1,167 cells	43 ROI 16,850 cells	22 ROI 4,084 cells	34 ROI 5,892 cells
Cerebellum, ML	41 stacks 361 cells	26 stacks 179 cells	42 ROI 3,982 cells	23 ROI 1,313 cells	35 ROI 1,632 cells
Cerebellum, WM	32 stacks 138 cells	28 stacks 105 cells	29 ROI 1,746 cells	15 ROI 778 cells	23 ROI 831 cells
Total	454 stacks 17,672 cells	413 stacks 14,598 cells	334 ROI 119,106 cells	201 ROI 39,808 cells	215 ROI 37,292 cells

Table 1: Numbers of cells, stacks and ROIs analyzed in each of ten structures of interest in the mouse brain. CerCx, cerebral cortex; GM, gray matter; WM, white matter; GL, granular cell layer; ML, molecular cell layer.

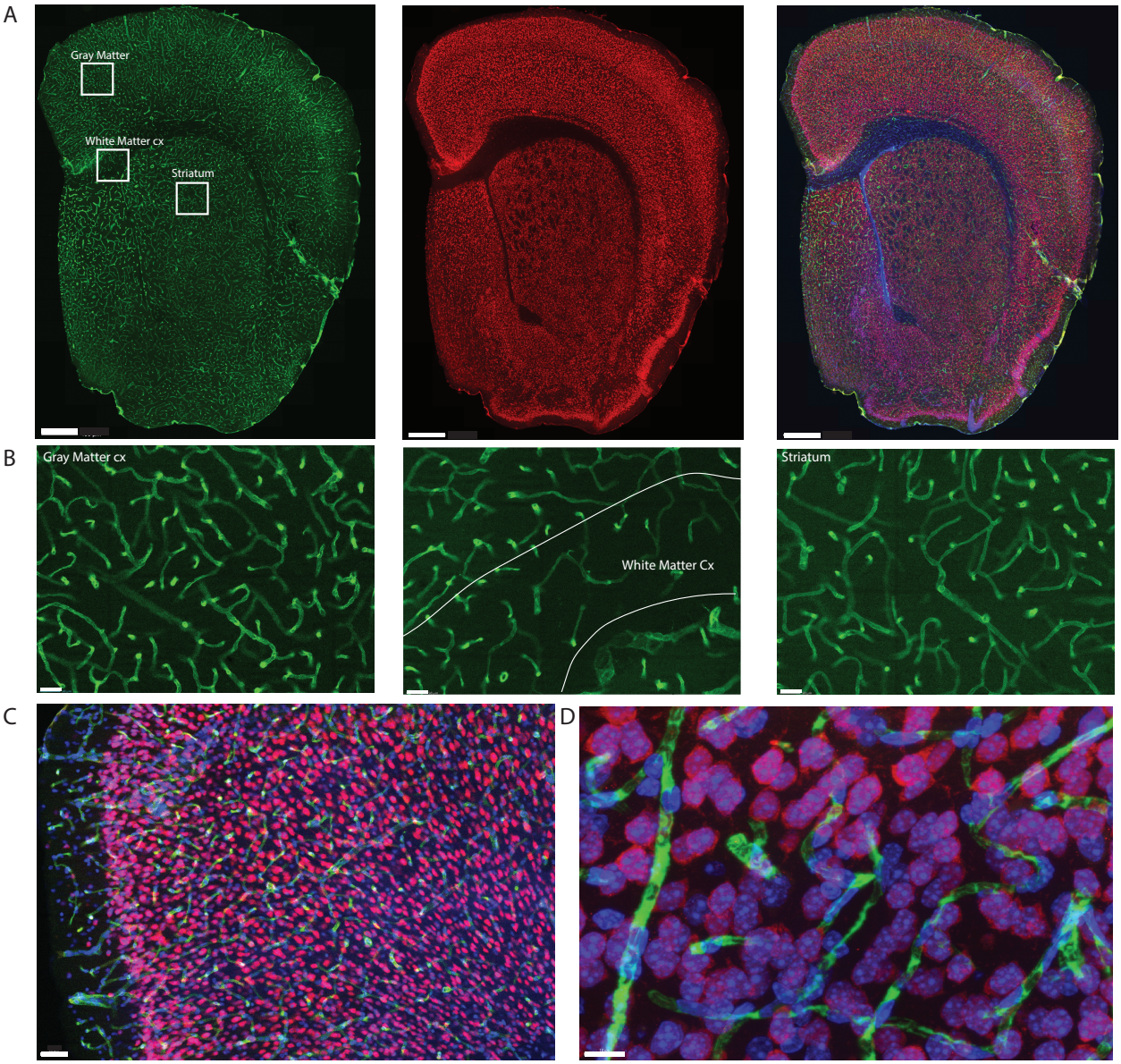

Figure 1. Example of triple labeling for vasculature, neurons, and all cell nuclei. Shown is a coronal section of a mouse brain label by systemic injection of FITC-Dextran. A. Coronal section of mouse brain showing microvasculature labeled with injection of FITC-dextran (left, green), neuronal nuclei labeled with NeuN-Cy3 (center, red), and all nuclei labeled with DAPI (right, blue in merged images). Scale bar, 400µm. **B.** Zoom of insets in A using the 63x objective with the thinner depth of field illustrating the extent of differences in capillary densities across brain sites. Scale bar, 50 µm. **C.** Section through cortical gray matter under 20x magnification stained to reveal Collagen IV (green), NeuN (red) and cell nuclei (blue). Scale bar, 50 µm. **D.** Maximal projection image of 3D stack through cortical gray matter imaged under 63x magnification. Scale bar, 10µm.

From all DAPI-labeled cell nuclei in each stack or 2D ROI, we identified all NeuN-positive cell nuclei as neurons; all nuclei directly associated with collagen IV-labeled or FITC-dextran filled capillaries as endothelial and associated cells (which includes eventual pericytes; heretofore, "endothelial cells"), and by elimination, all remaining nuclei were deemed glial cells (Fig. 2). Cell densities were calculated as cell nuclei per mm^3 or mm^2, depending on the stack volume or ROI area analyzed to include capillaries only. All results are shown side by side in 2D and 3D analyses.

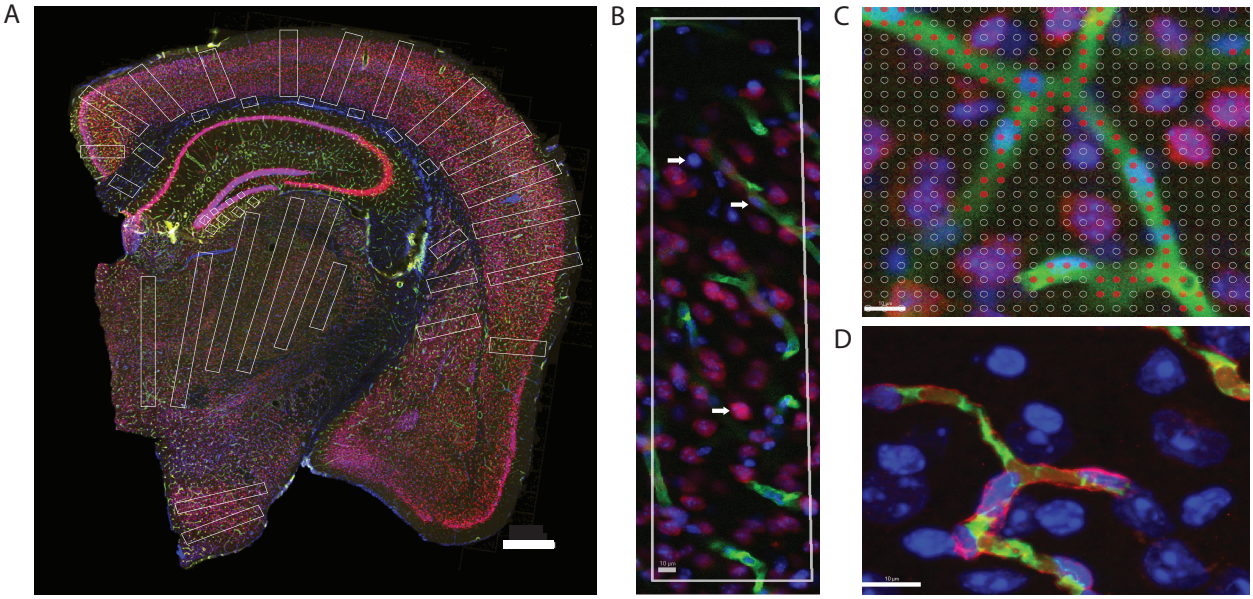

Figure 2. Two-dimensional image analysis. A. Areas sampled for 2D quantification are shown in white across structures in a coronal section of the mouse brain. Scale bar, 500 µm. **B.** ROI in the cortical gray matter showing microvasculature labeled with anti-collagen IV (green), neurons labeled with anti-NeuN (red) and Dapi to reveal all cell nuclei (blue). Cell nuclei appearing inside green-labeled blood vessels are considered capillary-associated nuclei; cell nuclei double-labeled in red are considered neuronal cell nuclei; all remaining nuclei are identified by exclusion as glial cell nuclei. **C.** A Cavalieri estimator grid of 4 µm spacing (shown) was applied to images acquired under 20x magnification, and a 2µm grid was applied to images acquired under 63x magnification. The points marked in red correspond to the area of the image occupied by capillaries. Scale bar, 10µm **D**. Superposition of FITC-dextran (green, lumen) and collagen IV (red, basal lamina) labeling of capillaries. Single image acquired under 63x magnification. Scale bar, 10µm.

175 **Experimental animals:** Five male Swiss mice aged 2.5 months were analyzed. Two mice
176 received an injection of 200 mg/kg of fluorescein-isothiocyanate-dextran (FITC-dextran 70 kDa)
177 in the caudal vein, to label the lumen of all blood vessels (Fig. 2). One hour after the injection,
178 the half-life required for distribution in the lumen of blood vessels (Wang et al., 2016), the
179 animals were deeply anesthetized with Xylazine (15 mg/Kg) and Ketamine (100 mg/Kg),
180 decapitated, and their brain was quickly removed and fixed by immersion in 4% of
181 paraformaldehyde in phosphate buffer for one hour followed by 30% sucrose in 0.1 M phosphate
182 buffer for cryoprotection. Using a Leica microtome, the cerebellum was cut into a series of 40
183 µm thick sagittal sections, and the remaining tissue was cut into a series of 40 µm coronal
184 sections. All sections were stored at -20°C in antifreeze solution (30% polyethylene glycol and
185 30% glycerol in 0.1 M phosphate buffer) until further use. Three other mice were similarly
186 deeply anesthetized with Xylazine and Ketamine and perfused through the heart with 0.9% saline
187 followed by 4% paraformaldehyde in phosphate buffer. The brain was removed and post-fixed
188 for one hour by immersion in 4% of paraformaldehyde in phosphate buffer, then sectioned as
189 above.

190 **Immunofluorescence:** One in every six sections of each brain was subjected to
191 immunohistochemistry and counterstaining with DAPI. Anti-NeuN antibody was used to reveal
192 neurons; additionally, those sections from the three animals not injected with FITC-Dextran were
193 subjected to immunohistochemistry against collagen IV to reveal cell nuclei intimately
194 associated with capillaries (Fig.2)

195 Each section was washed in phosphate buffer (PB) for five minutes, heat for one hour at
196 70 °C in a 0.1 M solution of boric acid, pH 9.0, then incubated for one hour in PB containing 3%
197 normal goat serum (Sigma-Aldrich, LG9023) and 2% bovine serum albumin (Sigma-Aldrich-

198 A2058). Sections from animals not injected with FITC-Dextran were next incubated under
199 stirring for 48 hours at 4°C in PB containing rabbit polyclonal anti-collagen IV antibody
200 (Abcam, Ab6586) at a 1:500 dilution. Each section was then washed three times in PB for 5
201 minutes each and incubated for 2 hours at 4°C in a 1:500 dilution of Alexa Fluor 488 goat anti-
202 rabbit secondary antibody (Abcam, Ab150077). From this step on, all brain sections were treated
203 similarly: washed three times in PB and incubated for 24 hours at 4°C under continuous stirring
204 with rabbit primary polyclonal antibody against Cy3-conjugated NeuN (Millipore, ABN78C3)
205 diluted 1:1000 in PB. All sections were then labeled with DAPI (4',6-Diamidino-2-Phenylindole
206 Dilactate, from stock solution at 20 mg/l) to provide counter-staining for identification of brain
207 structures and allow visualization of all cell nuclei in each section. The sections were then
208 mounted on glass slides and coated with Vectashield (Vector Labs, Cat. number H-1400) for
209 viewing under fluorescence microscopy.

210 **Structures analyzed:** The ten structures of interest targeted for analysis (gray matter (GM) and
211 white matter (WM) of the cerebral cortex; striatum; thalamus; hypothalamus; granular and
212 molecular layers of the hippocampal dentate gyrus; white matter and granular and molecular
213 layers of the cerebellum) were defined according to the Mouse Brain Atlas (Franklin and
214 Paxinos, 1997).

215 **Microscopy:** Two Zeiss AxioImager M2 microscopes equipped with an Apotome 2 for confocal
216 imaging under structured illumination (Carl Zeiss, Jena, Germany) and driven by
217 StereoInvestigator software (Microbrightfield Bioscience, Williston, VT) were used for all image
218 acquisition.

219 We first delineated the boundaries of the ten brain structures of interest in each section.
220 For each structure, image stacks for 3D analysis were acquired using systematic random

221 sampling in Stereo Investigator under magnification with a 63x objective (Plan-ApoChromat),
222 which gives a depth of field of 0.5 µm with oil, with an optical plane of 0.5 µm and step size of
223 0.5 µm. Stacks were 1388 x1040 µm wide x 30 µm thick and typically contained 60 images
224 each, spanning most of the full mounted thickness of the section. Within each stack, 3D counting
225 probes placed were variable in size according to the structure (Table 2) and were placed to
226 exclude the sectioned surfaces and zones outside the structure of interest. The grey matter of the
227 cerebellar cortex was imaged as a whole and analyzed separately into molecular and granular
228 layers. For 2D analysis, image composites of the entire brain sections were acquired under 20x
229 magnification (EC Plan-NeoFluar/420350-9900), which gives a thicker depth of field of ca. 4
230 µm, and counting probes consisted of rectangular regions of interest (ROIs) placed to cover large
231 areas of the target structures in each brain section (see Fig. 2). In the cerebral cortex, rectangular
232 probes spanned the entire grey matter from pia to the white matter border, and 5-15 probes of ca.
233 800 µm width were placed at regular intervals along each section. For all other structures, 2-8
234 rectangular probes were placed in each section, seeking to maximize the sampled surface of each
235 structure (Fig. 2A).

236

CerCx GM	X 127 y 96 z 20 µm
CerCx WM	x 80 y 75 z 20 µm
Thalamus	x 100 y 95 z 20 µm
Hypothalamus	x 100 y 95 z 20 µm
Striatum	x 100 y 95 z 20 µm
Hippocampus ML	x 40 y 40 z 20 µm
Hippocampus GL	x 30 y 30 z 20 µm
Cerebellum GK	x 40 y 40 z 20 µm
Cerebellum ML	x 40 y 40 z 20 µm
Cerebellum WM	x 40 y 40 z 20 µm

237
238 **Table 2: Size of 3D counting probes per structure.** CerCx, cerebral cortex; GM, gray matter; WM, white matter;
239 GL, granular cell layer; ML, molecular cell layer.

240

241

242 Although highly time-consuming, detailed analysis of 3D images was performed first to
243 rule out bias in data acquisition due to any preferential organization of capillaries relative to the
244 plane of section, given the three-dimensional nature of the distribution of the capillary network.
245 To ensure feasibility of future analyses of a large number of species, and to allow for a much
246 larger sample size, we compared the results of the 3D analysis of small image stacks with the
247 much faster and more practical analysis of 2D image composites, which permitted the analysis of
248 much larger ROIs and numbers of cells in half as much time. Those analyses had to be
249 performed in separate animals due to bleaching of the immunofluorescence during acquisition of
250 image stacks. Due to software limitations that precluded acquiring large composites at 63x, 2D
251 image composites had to be acquired at 20x, which leads to inflated estimates of area (or
252 volume) fraction occupied by capillaries due to the projection of oblique vessels given the larger
253 thickness of the optical sections at 20x (ca. 4 μm) compared to 63x (ca. 0.5 μm). For the same
254 reason, estimates of local cell densities will also differ between the two methods. However, we
255 hypothesize that all relationships across variables should remain unaffected by the method of
256 image acquisition. All results are thus presented side by side for 3D and 2D analyses. Data points
257 overlap across animals (shown in different symbols in all figures), and are thus analyzed jointly.

258 **3D analysis:** Stacks in the targeted brain structures of two FITC-injected mice were acquired
259 using systematic random sampling (SRS) of each structure in each of 1 of 6 sections. From each
260 brain, 13 and 18 sagittal sections through the cerebellum and 24 and 23 coronal sections through
261 the remaining brain structures, including the cerebrum, were analyzed. A total of 867 stacks were
262 analyzed across the ten brain structures in two mice (Table 1, mouse 01 and mouse 02).

263 **2D analysis:** From each of three animals, 21, 12 and 17 sections through the cerebellum and 21,
264 20 and 14 sections through the remaining brain structures were analyzed. A total of 750 ROIs
265 were imaged and analyzed across the ten brain structures (Table 1, mice 03-05).

266 **Image analysis:** In each stack and ROI analyzed, we manually identified each DAPI-stained cell
267 nucleus in the structure site as neuronal (when it expressed NeuN immunoreactivity), endothelial
268 or belonging to other capillary-associated cells (when the cell was intimately associated with
269 FITC-labeled capillary lumen or collagen IV-stained basal lamina, which includes pericytes), or
270 glial (by exclusion; Fig. 2B).

271 Microvascular area fraction (hereafter termed "capillary area fraction" for simplicity) was
272 estimated in image stacks and 2D ROIs using the Cavalieri estimator in StereoInvestigator using
273 a grid of points separated by 2 μm in 3D images and 4 μm in 2D images (Figure 2C). Capillary
274 *area* and *volume* fraction are interchangeable (25) and refer to the fraction of tissue formed by
275 endothelial cells and the lumen of the capillaries that they form. In order to restrict analysis to
276 capillaries, where stacks included large vessels, the counting probe was reduced to avoid it, or
277 else the stack was discarded. In 2D, ROIs were placed to avoid large vessels.

278 Labeling capillaries with FITC-dextran or immunohistochemistry to collagen IV is
279 expected to lead to slightly different measurements of capillary density expressed as area (or
280 volume) fraction, because while the former labels the lumen of blood vessels, the latter labels the
281 basal lamina of the cells that form the walls of the vessels. However, estimates of numbers of
282 capillary-associated cells per site should remain unaffected. To evaluate how much the
283 difference in measured capillary volume fraction depending on staining method would impact
284 our results, one additional 1-in-6 series of brain sections of mouse #01, which received the
285 injection of FITC-Dextran, were double-labeled for collagen IV using the same primary antibody

286 as before, but a different secondary antibody, conjugated to Alexa Fluor 546 (1:500/#A11010 -
287 Life). Fig. 2D illustrates the coincident but non-overlapping double labeling of lumen and basal
288 lamina of the microvasculature and the associated DAPI-stained cell nuclei. Quantification of the
289 area fraction covered by capillaries in 2D composites acquired at 20x showed a detectable but
290 not statistically significant difference between the vascular fraction estimated with collagen IV
291 (7.4±0.3%) compared to FITC-Dextran (6.6±0.4%).

292 **Correlations with synaptic density:** In order to determine whether local densities of synapses
293 correlate with local densities of neurons and capillaries and to establish how variable are the
294 ratios of synapses per neuron and number of synapses supplied per capillary cell, we proceeded
295 with the quantification of four sections from the brain of mouse #4 that matched the respective
296 levels of the four coronal sections through the cerebral cortex of one individual mouse in the
297 synaptome study of Zhu et al. (2018). We used the Mouse Brain Atlas (Franklin and Paxinos,
298 1997) to place large ROIs in the same structures. 2D composite images acquired under 20x
299 magnification were analyzed to determine the density of cells and vascular fraction of neocortex
300 in our images for comparison with the total number of synapses labeled with either PSD95 or
301 SAP (Zhu et al. 2018).

302 **Statistical analysis:** All analyses were performed in JMP14 PRO, using non-parametric
303 Spearman correlation coefficients to test the correlation between variables, and regression to
304 mathematical functions to determine the type of relationship between variables.

305

306

307

Results

To guide the interpretation of our findings, the three main possible scenarios are depicted in Figure 3. The top row illustrates the results expected if steady-state capillary density in the adult brain reflected local variations in neuronal density, and the average neuron used similar amounts of energy regardless of its size or location. In this case, local capillary density should be directly proportional to local neuronal density, and energy availability per neuron, indicated by the ratio of endothelial-associated cells per neuron, should remain constant across brain sites. On the other hand, if larger neurons use more energy, then sites with larger neurons and thus lower neuronal densities should have higher E/N (Figure 3, rows 2 and 3). However, this finding could occur in either one of two other scenarios, depending on whether higher E/N where it happens is due to reorganization of the capillary bed reflecting neuronal *demand*, in which case larger capillary densities would be expected in those sites with larger neurons (and therefore lower neuronal densities; row 3), or is imposed by a lack of variation in capillary density across brain sites (row 2). The three particular cases in which numbers of synapses are constant per volume (left), constant per neuron (center) or larger in larger neurons (right) are depicted separately for each scenario and illustrate the ensuing expected variation in energy availability per synapse as well as how energy availability per neuron would vary together with energy availability per synapse or not.

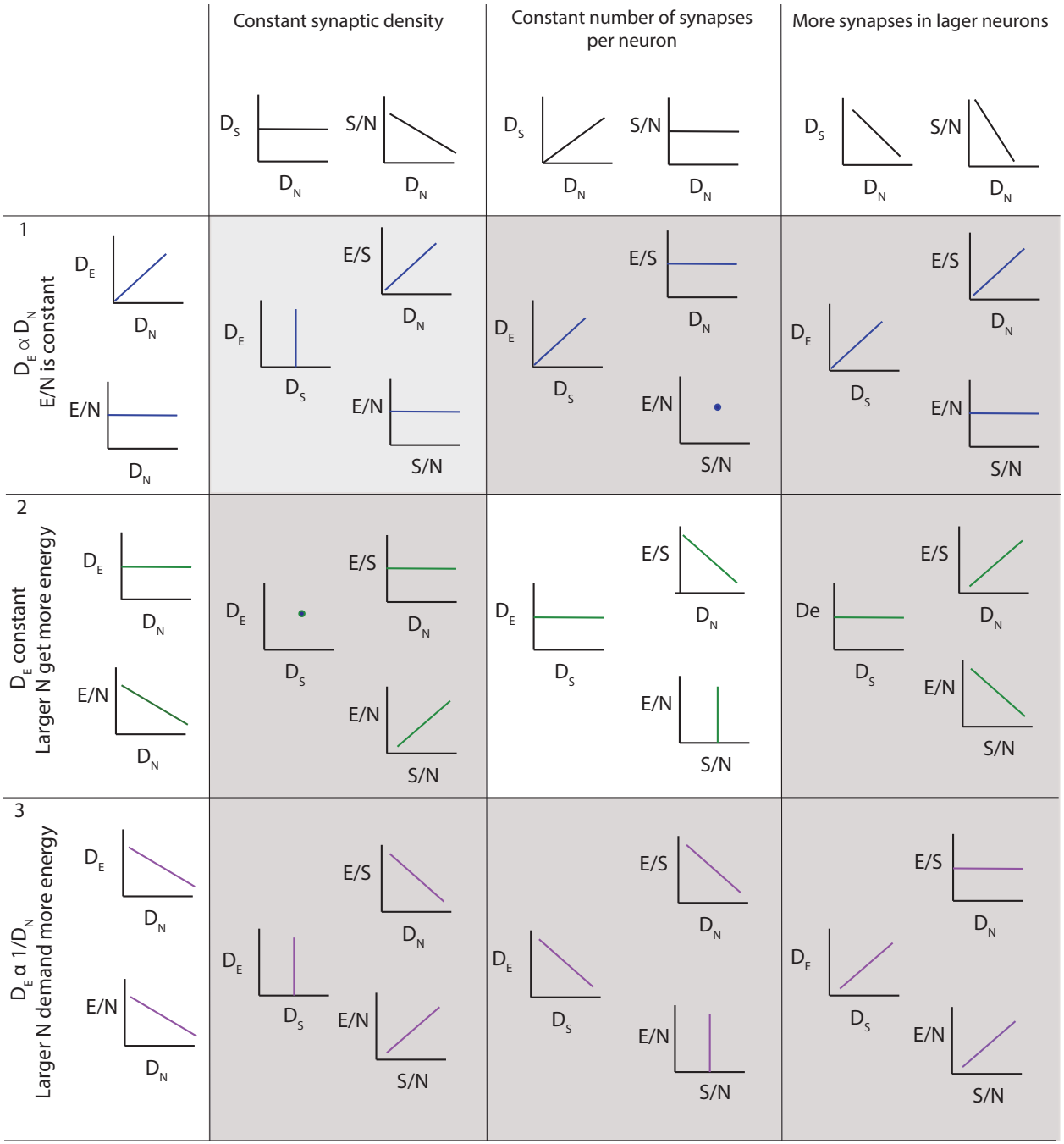

Figure 3. Three of several possible scenarios of relationships among local density of capillary cells (D_E), local density of neurons (D_N), energy available per neuron (E/N, estimated as D_E/D_N), local density of synapses (D_S), average number of synapses per neuron (S/N) and average energy supply per synapse (E/S). Scenario 1 (top row): neurons demand a certain fixed supply of energy, and the capillary bed adjusts to supply it at a steady-state, such that energy supply per neuron is constant across sites. In this scenario, D_E is expected to be proportional to D_N, and energy available per neuron (E/N) is constant. **Scenario 2 (second row)**: capillary supply to brain tissue is constant across sites, and neurons compete for whatever energy is available. In this case, D_E is expected to be

relatively constant regardless of local D_N; as a result, E/N is larger in sites of lower neuronal densities (indicative of larger neurons), where fewer neurons compete for a limited supply of energy. This is the scenario supported by our findings, but incompatible with current models. **Scenario 3 (third row)**: larger neurons demand more energy, and the capillary bed adjusts to supply it, such that energy supply per neuron is larger where neurons are also larger, and thus occur at lower D_N. This scenario is compatible with current models, but is not supported by our present findings. **Columns** indicate, for each scenario of capillary and neuronal distribution, the expected findings regarding variations across the variables measurable in this study depending on whether **(left column)** local synaptic densities are mostly constant across sites, such that there are more synapses per neuron where neurons are larger (and D_N lower); **(center column)** the number of synapses per neuron is mostly constant, such that there are more synapses where there also are more neurons; and **(right column)** larger neurons have many more synapses than smaller neurons, such that local synaptic densities are larger where neurons are larger (and D_N lower). Our findings support a constant density of capillaries with fairly constant densities of synapses per neuron, such that energy supply both per neuron and per synapse, and thus energy availability per neuron and per synapse, decreases the higher the local neuronal density, that is, the smaller the average local volume of individual neuronal cells. This is the scenario highlighted in the center panel.

Across the ten brain structures examined, we find that the capillary area fraction is very small, amounting to no more than 3% of the tissue in any structure in 3D image stacks. While individual measurements of local capillary fraction vary 10x-fold across all brain sites, the average capillary fraction per structure varies only about 2-fold across structures, with 95% of measurements ranging around 1.29 ± 1.39% (Table 3). The average capillary fraction is highest in the gray matter of the cerebral cortex (2.22±0.11%), and lowest in the granular layer of the dentate gyrus and subcortical white matter (0.70±0.07%; Table 3). In 2D images, we found similarly small variation in capillary fraction, as well as lower capillary fractions in white matter than in gray matter, despite the artificially higher nominal capillary fractions measured with this method due to the larger optical thickness of the images (Table 4). The capillary fractions we report in 3D analyses are similar to vascular fractions between 2% and 6% reported in the mouse cerebral cortical grey matter (Tsai et al., 2009) and between 2.1% and 3.1% in the cat, macaque and human gray matter cortex (Boero et al., 1999; Pawlik et al., 1981; Lauwers et al., 2008).

362

363 **Table 3. Fractional cellular composition of different structures of the mouse brain, quantified in 3D.** Values
364 correspond to the average across sites in each structure of two mice (#1 and #2). CerCx, cerebral cortex; GM, gray
365 matter; WM, white matter; GL, granular cell layer; ML, molecular cell layer; Cb, cerebellum.
366

3D	% capillary fraction	% endothelial cells	% neurons	% glial cells	Glial cells % of non-neuronal cells
CerCx, GM	2.22 ± 0.11%	13.90 ± 0.79%	57.86 ± 1.53%	28.22 ± 1.23%	66.64 ± 1.49%
CerCx, WM	0.75 ± 0.03%	7.62 ± 0.60%	5.75 ± 1.15%	82.61 ± 1.41%	91.37 ± 0.76%
Striatum	1.43 ± 0.06%	7.94 ± 0.34%	62.47 ± 1.10%	29.57 ± 1.10%	77.58 ± 0.99%
Thalamus	1.35 ± 0.05%	10.74 ± 0.52%	51.24 ± 1.31%	38.01 ± 1.2%	77.31 ± 1.00%
Hypothalamus	1.34 ± 0.06%	10.14 ± 0.69%	60.62 ± 1.61%	29.23 ± 1.36%	73.34 ± 1.64%
DG, GL	0.70 ± 0.07%	1.46 ± 0.47%	94.96 ± 1.08%	3.57 ± 0.92%	67.46 ± 9.30%
DG, ML	1.10 ± 0.06%	29.18 ± 3.21%	10.33 ± 3.29%	60.48 ± 3.29%	68.23 ± 3.35%
Cb, GL	1.56 ± 0.06%	2.58 ± 0.33%	95.44 ±0.46%	1.96 ±0.33%	38.86 ± 5.06%
Cb, ML	1.69 ± 0.09%	13.92 ± 3.76%	59.77 ± 3.90%	26.30 ± 3.76%	54.35 ± 4.93%
Cb, WM	1.25 ± 0.06%	14.14 ± 2.68%	0.73 ± 0.52%	85.12 ± 2.76%	85.64 ± 2.69%

367
368
369 **Table 4. Fractional cellular composition of different structures of the mouse brain, quantified in 2D.** Values
370 correspond to the average across sites in each brain structure of three mice (#3, #4 and #5). *Note that the capillary
371 fraction appears higher here than when measured in 3D due to the deeper focal thickness under the lower
372 magnification used for 2D image acquisition, which artificially inflates the relative capillary fraction. Other values
373 are similar between 2D and 3D estimates.
374
375

2D	% capillary fraction*	% endothelial cells	% neurons	% glial cells	Glial cells % of non-neuronal cells
CerCx, GM	8.65 ± 0.21%	14.37 ± 0.23%	60.86 ± 0.39%	24.75 ± 0.36%	63.06 ± 0.53%
CerCx, WM	5.35 ± 0.27%	10.63 ± 0.55%	2.99 ± 0.93%	86.37 ± 1.18%	88.55 ± 0.75%
Striatum	7.74 ± 0.25%	11.88 ± 0.37%	63.59 ± 0.83%	24.51 ± 0.71%	67.14 ± 0.88%
Thalamus	7.58 ± 0.71%	14.53 ± 0.71%	45.88 ± 1.89%	39.57 ± 1.90%	72.19 ± 1.30%
Hypothalamus	7.28 ± 0.39%	12.38 ± 0.63%	57.13 ± 1.60%	30.47 ± 1.34%	70.77 ± 1.40%

DG, GL	6.17 ± 0.06%	4.55 ± 0.72%	90.89 ± 1.46%	4.55 ± 0.89%	46.32 ± 5.72%
DG, ML	10.91 ± 0.91%	30.67 ± 1.70%	13.17 ± 2.34%	56.15 ± 2.34%	64.43 ± 1.93%
Cb, GL	6.76 ± 0.26%	3.02 ± 0.17%	91.00 ± 0.47%	5.97 ± 0.38%	63.22 ± 1.83%
Cb, ML	7.20 ± 0.25%	18.77 ± 0.62%	47.02 ± 1.57%	34.20 ± 1.48%	62.47 ± 1.48%
Cb, WM	4.16 ± 0.22%	13.50 ± 0.77%	2.34 ± 0.56%	84.14 ± 0.95%	86.13 ± 0.79%

Interestingly, capillary-associated ("endothelial") cells typically constitute between 7 and 14% of all cells forming the brain structures examined (Tables 3, 4), a much larger percentage than could be expected from the average vascular fraction of 0.7-2.2% of the 3D volume that they occupy. This discrepancy indicates that endothelial cells are, on average, much smaller than neurons and glial cells in the tissue. Still, glial cells are consistently the majority (at least 60-70%) of non-neuronal cells in all structures (Tables 3, 4). As expected from our previous studies (reviewed in Herculano-Houzel et al., 2014), the percentage of cells that are neurons is highly variable across structures and sites within a structure; neurons are the vast majority of all cells in the granular layers of the dentate gyrus and cerebellum, a smaller percentage of all cells in other gray matter structures, and rare (but present) within the subcortical white matter of both cerebral and cerebellar cortices (Tables 3, 4).

As expected for two different measurements of the same feature (capillary density), local endothelial cell density correlates well with local capillary area or volume fraction within and across the different brain structures, as well as across animals, especially in the 2D sample, which included a much larger number of sites and cells (Fig. 4A; Table 1). Both capillary fraction and local endothelial cell density vary by a single order of magnitude across sites in the mouse brain, whether measured in 2D or 3D (Fig. 4A). The two capillary density-related variables are correlated within each structure individually (Table 5), and there is good overlap in

data points across structures and animals, especially in the larger 2D dataset (Fig. 4A, right), where the overlapping power relationships (Table 5) indicate that the relationship between capillary fraction and cellular composition of capillaries is shared throughout the brain. This agreement suggests that endothelial cell density is a good proxy for the resting rates of blood flow and glucose use (Klein et al., 1986; Noda et al., 2002).

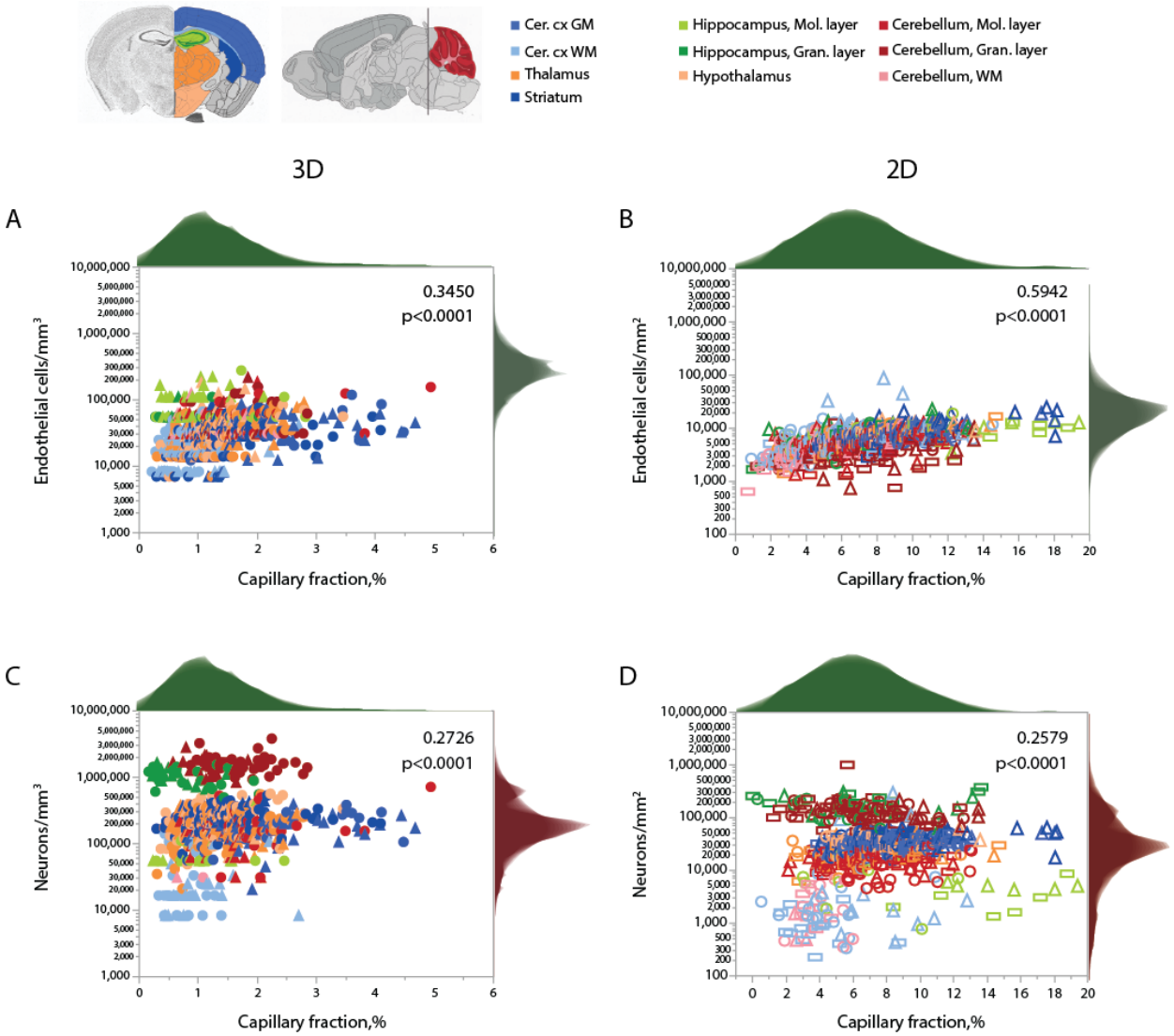

Figure 4: Local capillary fraction correlates with local endothelial cell density, but not with neuronal cell density. A, B: Local density of endothelial cells correlates with local vascular fraction across all sites and structures analyzed in 3D (**A**; two animals, shown in circles or triangles, left) and in 2D (**B**; three animals, shown in circles, triangles, or rectangles, right) with the Spearman correlation coefficients and p-values across all animals and sites indicated in each graph. **C, D:** In contrast, local neuronal density does not correlate significantly with local vascular

fraction across brain sites and structures in 3D (**C**) or in 2D (**D**). Histograms above and to the right reflect the distribution of all data points in each axis. Graphs in **A/C** and **B/D** are shown with similar X and Y scales for comparison. Correlation coefficients and power exponents for each structure are given in Table 5.

Neuronal densities, in contrast, vary over two orders of magnitude across sites in gray matter structures, from 31,250 to 3,843,750/mm^3 (Fig. 4B), and are not significantly correlated with local capillary fraction (Figure 4B) across brain sites and structures. In fact, brain structures with enormously different neuronal densities have capillary fractions in the same restricted range (Fig. 4B), and correlations, where significant, can be positive (cortical GM) or negative (cerebellar granular layer; see Table 5 at end of document).

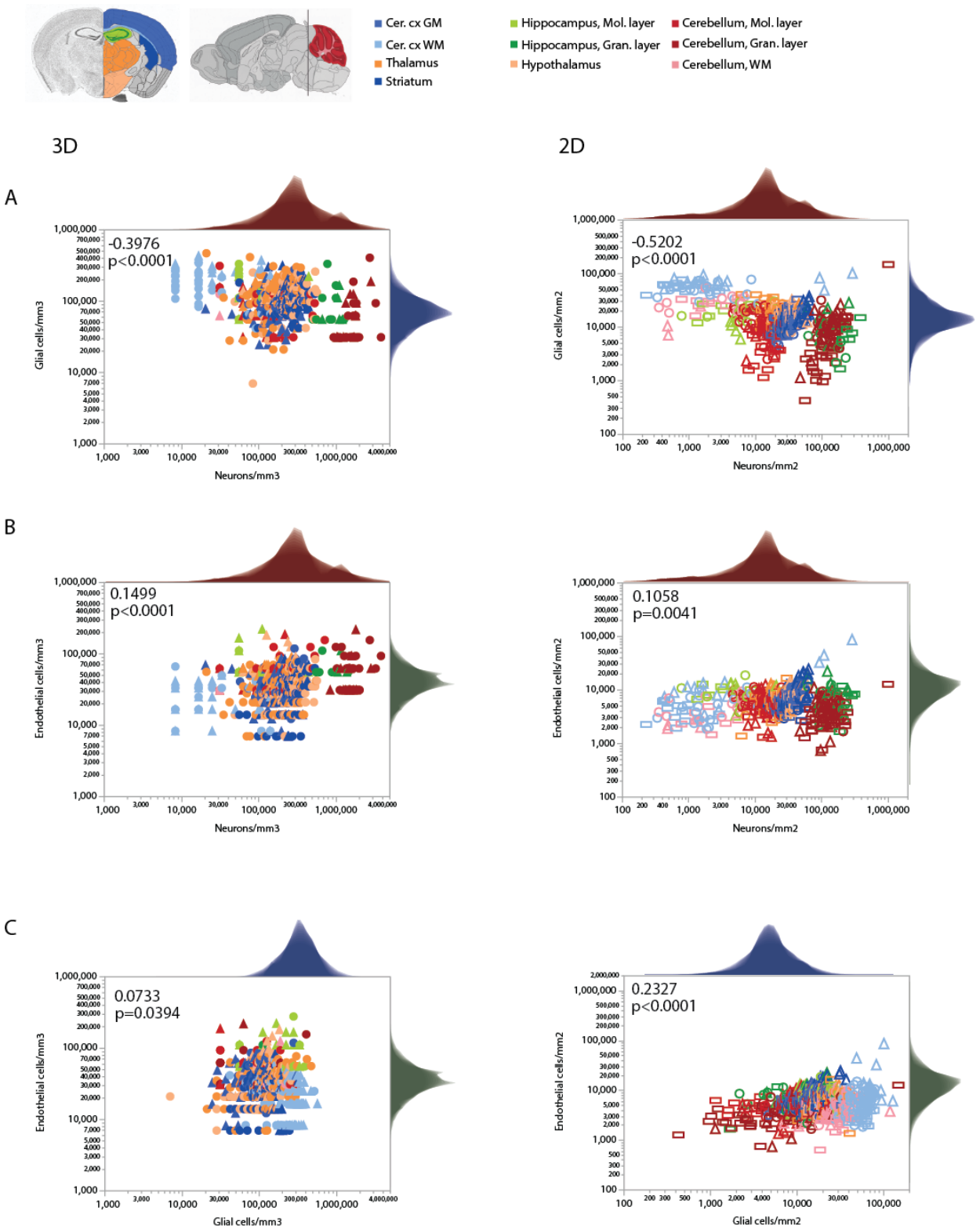

Figure 5. Local densities of different cell types vary concertedly only within some brain structures. Each plot is accompanied by the respective distribution histograms aligned with the X and Y axes. Spearman correlation coefficients and p-values across all structures and sites are indicated in each graph. **A.** Glial cell densities span just

421 over one order of magnitude across structures, while neuronal cell densities span two orders of magnitude. While the
422 correlation across all data points is significant and negative in both 3D and 2D datasets, analysis at that level ignores
423 obvious differences across structures (see Table 4). **B.** Similarly, endothelial cell densities are concentrated within
424 one order of magnitude across structures and sites, and are similar across structures with very different neuronal
425 densities. Still, local endothelial and neuronal cell densities are significantly and positively correlated within the
426 cortical gray matter, the thalamus, and the striatum (see Table 4). **C.** Glial and endothelial cell densities, which vary
427 little across sites and structures in comparison to neuronal densities, are not strongly correlated across brain
428 structures, and weakly correlated within some (see Table 5). All graphs are shown with similar X and Y scales for
429 comparison.
430

431 Like endothelial cell densities, variation in glial cell densities is restricted to within one order
432 of magnitude across sites in the mouse brain (Fig. 5A). Within the cortical gray matter, local
433 glial cell densities vary significantly in positive correlation with local neuronal density, as
434 previously observed across sites within both human (Ribeiro et al., 2013) and mouse (Herculano-
435 Houzel et al., 2013) cortices (Fig. 5A; Table 5). In contrast, there is no universal correlation
436 between local neuronal and glial cell densities across brain structures; if anything, there is a
437 modest negative correlation across all sites (Fig. 5A), which is due to the slightly more elevated
438 glial cell densities in white matter sites.

439 Importantly, a large range of neuronal densities occurs with fairly similar endothelial cell
440 densities across structures in the mouse brain, with only a weak overall trend toward higher
441 endothelial cell densities where neuronal densities are higher (Fig. 5B). A significant increase in
442 local endothelial cell density in sites with increasing local neuronal density is found only in the
443 cortical gray matter, thalamus and striatum (Fig. 5B, Table 5). Similarly, we find significant
444 correlations between local densities of endothelial cells and glial cells within some structures, but
445 no strong systematic correlation across locations (Fig. 5C).

446 Consistently with the larger variation of neuronal densities than glial cell densities across
447 locations, the glia/neuron (G/N) ratio is highly variable within the mouse brain, and is

448 universally and inversely related to local neuronal densities across all sites and structures (Fig.
449 6A, B). That is, there are more glial cells per neuron in those sites with lower neuronal densities,
450 in a relationship that applies both across and within structures, regardless of their identity (Table
451 S5). In contrast, the relationship between local glia/neuron ratio and glial cell density is specific
452 to each structure, with different ranges of glia/neuron ratios sharing similar glial cell densities
453 across structures (Fig. 6C, D). Importantly, although higher G/N ratios where neuronal densities
454 are smaller (and therefore neurons are larger) have been proposed to accompany the presumably
455 higher energetic demands of larger neurons (Attwell et al., 2001), the entire 10,000-fold range of
456 G/N ratios occurs within the same restricted range of endothelial cell densities, with no
457 consistent correlation across brain structures and sites (Figure 6E, F). That is, endothelial cell
458 densities are not significantly higher in those locations where each neuron is accompanied by a
459 larger number of glial cells.

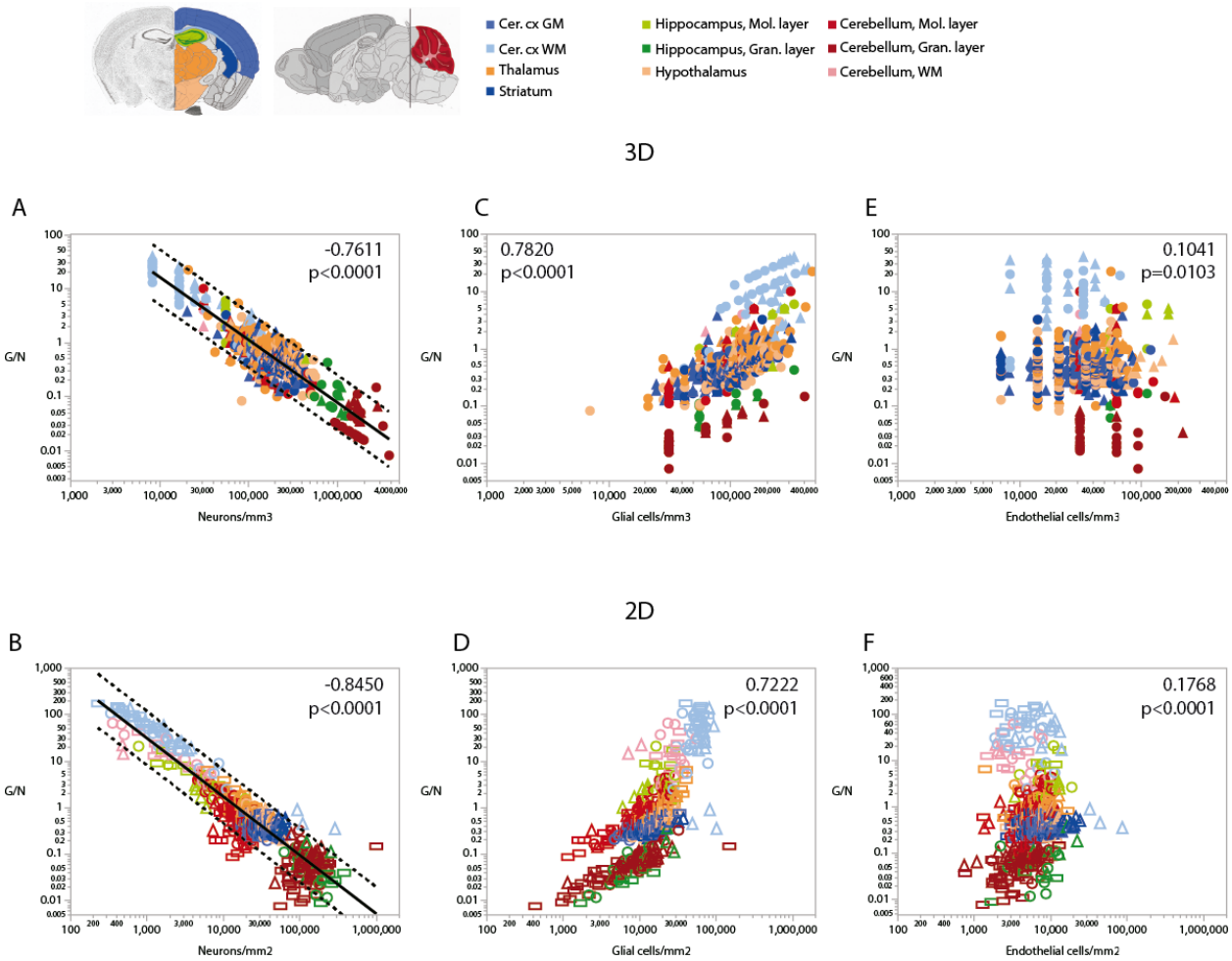

Figure 6. Ratio of glial cells per neuron (G/N) increases across brain structures and sites with decreasing neuronal densities. Spearman correlation coefficients and p-values across all structures and sites are indicated in each graph; relationships for each structure are given in Table 5. G/N ratios span over three orders of magnitude and vary as a single power function of neuronal density across all brain structures and sites whether measured in 3D stacks (**A**) or in 2D composite images **(B).** Power functions are plotted with 95% confidence interval (dashed lines), and have exponents -1.162±0.024, r^2=0.816, p<0.0001 (**A**, 3D) or -1.257±0.020, r^2=0.865, p<0.0001 (**B**, 2D). Notice that most data points in all structures are contained within the 95% CI of the function that applies across structures, indicating that the relationship is brain-wide. **C, D:** G/N ratio also correlates with glial cell densities across all brain structures and sites, but the relationships are clearly distinct across sites (see exponents in Table 5). **E, F:** Although a weak correlation is detected between G/N ratios and endothelial cell densities across brain structures and sites, most local correlations are non-significant or weak, with a wide range of non-overlapping values of G/N for similar endothelial cell densities across brain structures. All graphs are shown with similar X and Y scales for comparison.

Because of the much larger variation in neuronal densities than in endothelial cell densities across sites, the local ratio of endothelial cells per neuron is inversely proportional to local neuronal density across all sites and structures examined (Fig. 7). Importantly, this relationship is universal across brain locations, as the power function that applies across structures contains all structures and almost all data points within its 95% CI (Fig. 7A, B). That is, each neuron is accompanied by more endothelial cells at sites with lower neuronal densities than at sites with higher neuronal densities. In contrast, the ratio of endothelial cells per neuron does not vary consistently with local glial cell density neither across nor within brain structures (Fig. 7C, D). As expected for the quantity in the numerator of the ratio, local endothelial cell density is very strongly correlated with the E/N ratio in each brain structure in the mouse brain, but there is hardly any overlap across structures: because of the widely different neuronal densities across structures, brain sites with similar densities of endothelial cells have very different E/N ratios across structures (Fig. 7E, F). As could be expected of two quantities that are heavily dependent on variation in neuronal density, the E/N ratio is strongly and linearly correlated with the G/N ratio across all sites and structures (Fig. 8). That is, where more endothelial cells supply energy per neuron (i.e. in structure and sites with low neuron density), there are also more glial cells per neuron. Importantly, the relationship that applies across structures includes most data points for every structure, indicating that this relationship is universal.

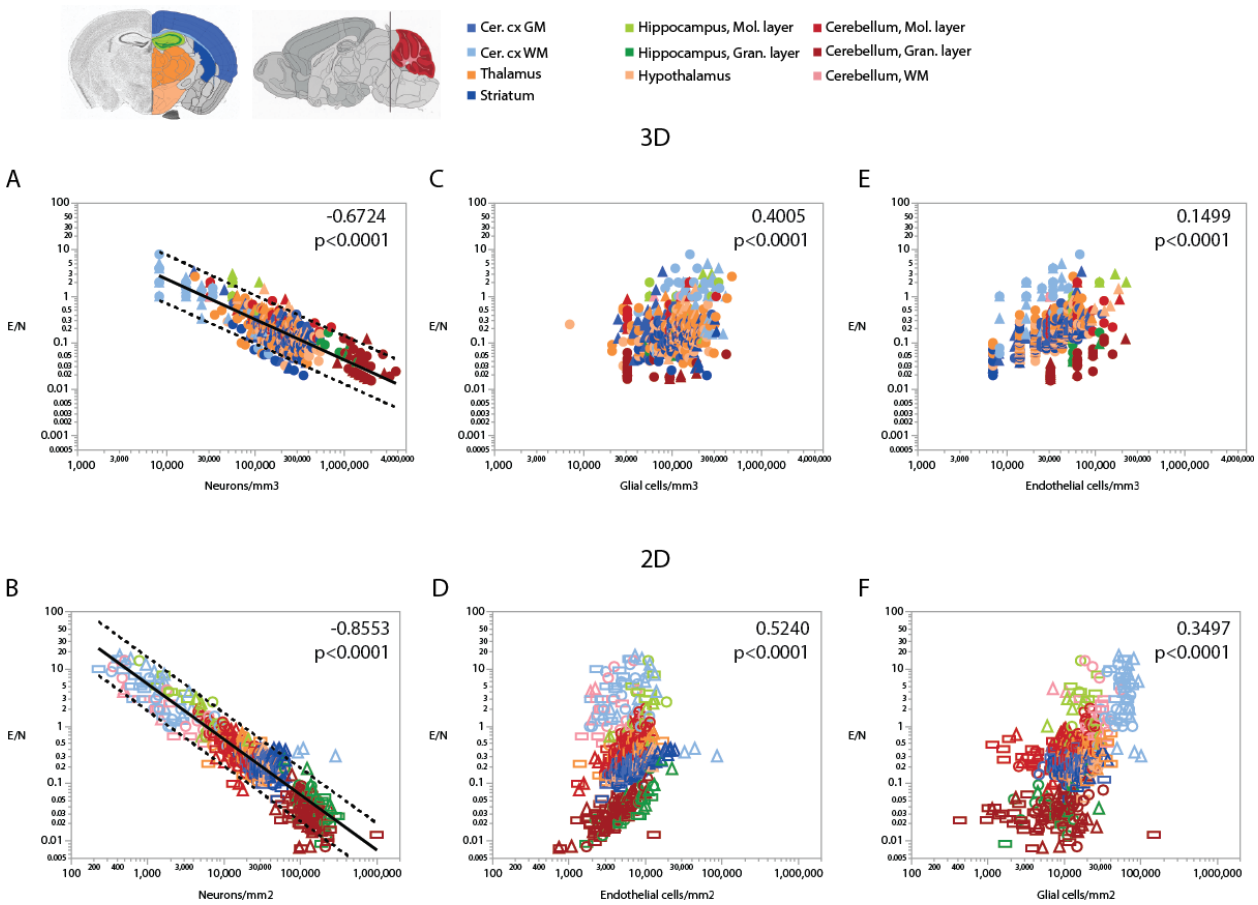

Figure 7. Ratio of endothelial cells per neuron (E/N) varies widely and uniformly across brain structures and sites depending on local neuronal density, but correlations with glial and endothelial cell densities only apply locally. Spearman correlation coefficients and p-values across all structures and sites are indicated in each graph; correlations and power function exponents for each structure are listed in Table 4. **A, B:** E/N ratios span three orders of magnitude across brain sites and structures and vary as a single power function of local neuronal density whether measured in 3D stacks (**A**) or in 2D composite images (**B**). **C, D:** E/N ratio appears to correlate with local glial cell density across brain structures in both datasets, but closer inspection reveals that the overall correlation results from the combination of locations and does not hold within most structures (see Table 5). **E, F:** In contrast, E/N ratios are strongly correlated with endothelial cell densities locally within each structure, but different brain structures have non-overlapping E/N ratios with similar endothelial cell densities, indicating that the apparent overall correlation does not result from a universal correlation, unlike that seen for the strong and universal correlation between E/N and neuronal density (**A, B**). All graphs are shown with similar X and Y scales for comparison.

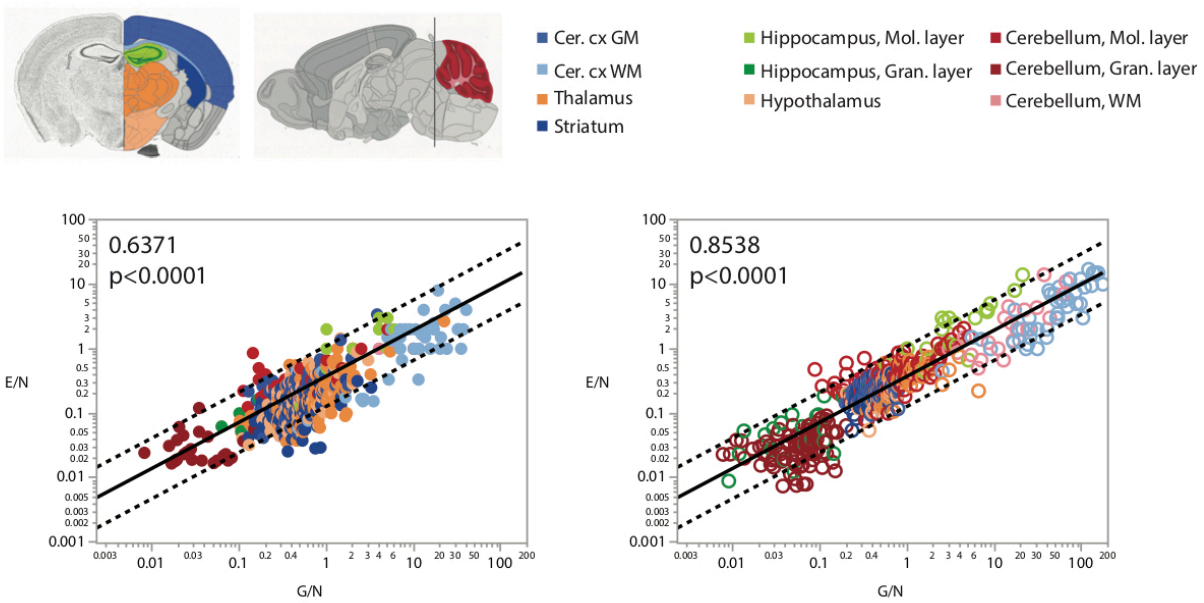

Figure 8. More endothelial cells per neuron (E/N) are uniformly found in brain structures and sites with more glial cells per neuron, as expected given that both these variables are strongly and inversely correlated with local neuronal density (Figs. 4, 5). Spearman correlation coefficients are indicated in the graphs.

Finally, comparing our measurements of local cell densities and capillary fraction in cortical grey matter sites matching those with recently published data on local synaptic densities in the mouse cerebral cortex (Zhu et al., 2018) we could examine whether there is evidence of higher energy availability in sites of higher synaptic densities to support the expectation that energy supply responds local demands due to synaptic activity (Attwell and Laughlin, 2001; Harris et al., 2012; Table 6). Densities of synapses (measured as synapses that express PSD and/or SAP according to data in Zhu et al., 2018) vary 1.5-fold across cortical sites, while densities of endothelial cells vary 2.5-fold and neuronal densities vary a similar 2.2-fold. However, we find no significant correlation between local endothelial cell density and synaptic density (Fig. 9A) or neuronal density (Fig. 9B) within the mouse cerebral cortex (Spearman, p=0.4133 and 0.7047), indicating that cortical sites with more synapses or more neurons receive as much capillary

521 supply as sites with fewer synapses or neurons. Higher local synaptic densities are modestly
522 associated with higher local neuronal densities (Fig. 9C; Spearman, p=0.0414), such that the
523 ratio of synapses per neuron is concentrated in the 6,500-9,500 range (Fig. 7E; Spearman, p=
524 0.0129 due to a single data point above 12,500), compatible with previous estimates of ca. 8,000
525 synapses per cortical neuron in the mouse (Schüz, and Palm, 1989; Braitenberg and Schüz,
526 1998). We find that the average number of synapses per neuron is not higher where there are
527 more synapses (Fig. 9D; Spearman, p=0.0775), and is also not significantly correlated with the
528 local number of glial cells per neuron (Spearman, p=0.3177; Table 6). Indeed, local densities of
529 synapses are not correlated with local glial cell densities (Spearman, p=0.6488), and the higher
530 the local glial cell density, the fewer the synapses per glial cell (Spearman rho=-0.831, p<0.0001;
531 Table 6). Crucially, the average number of synapses per neuron is not significantly correlated
532 with the local ratio of endothelial cells per neuron (Fig. 9F; Spearman, p=0.4717): the E/N ratio
533 varies about 4-fold across cortical sites with similar average numbers of synapses per neuron,
534 and at a similar capillary supply per neuron, local neurons may have more or fewer synapses on
535 average. Instead, the most striking pattern is, again, that at cortical sites where each neuron has
536 more capillary cells available to it, there are also more capillary cells available per synapse (Fig.
537 9G; Spearman, p=0.0001).
538

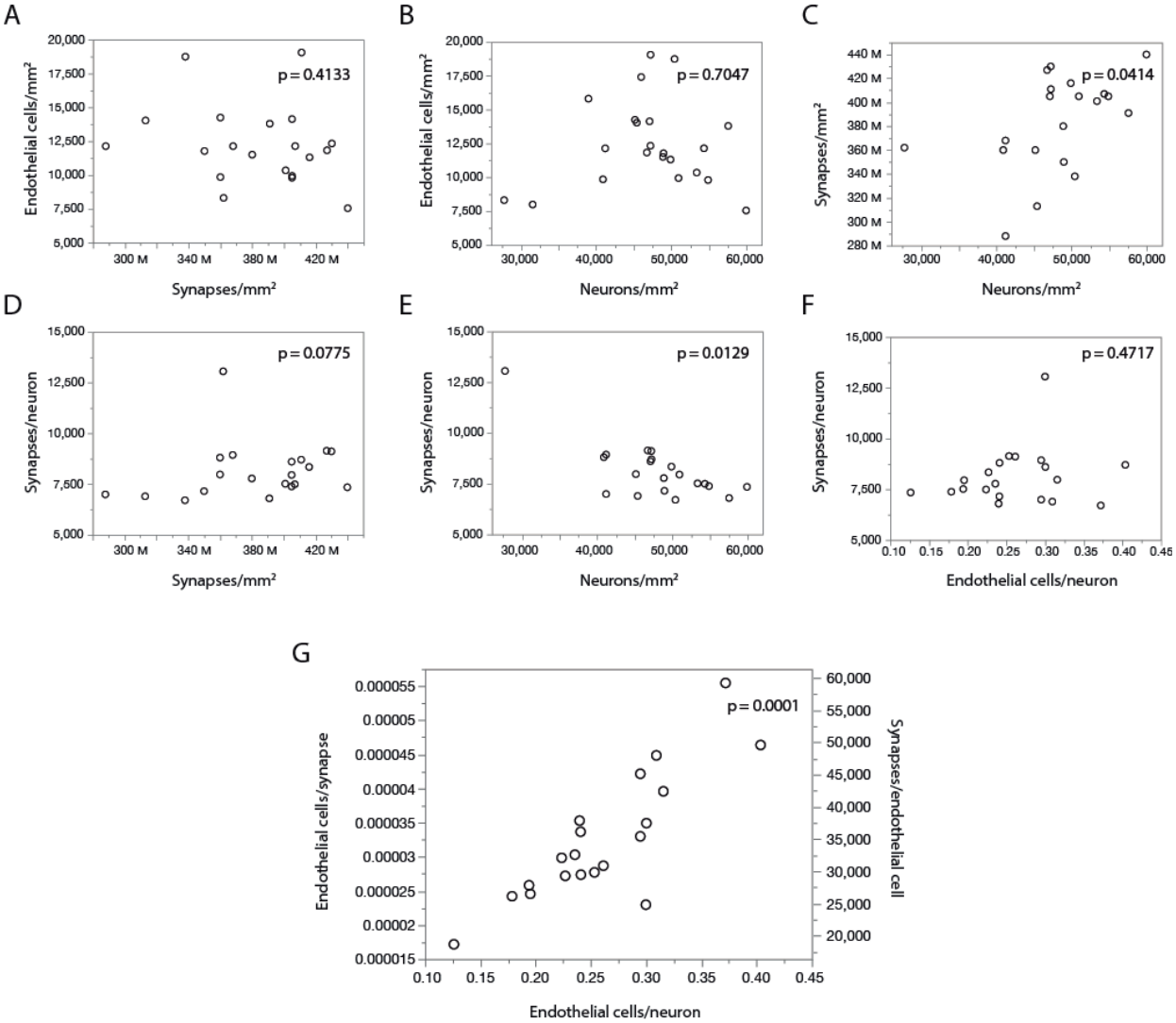

Figure 9. With fairly constant numbers of synapses per neuron, the number of synapses served per endothelial cell increases together with the ratio of endothelial cells per neuron across sites in the mouse cerebral cortex. Data on local synaptic densities from (Zhu et al., 2018) were combined to estimates of local densities of endothelial cells, neurons and glial cells in 2D images acquired in matching locations of the cerebral cortex as described in (Zhu et al., 2018). Local densities of endothelial cells are not significantly correlated with local synaptic densities (**A**) or neuronal densities (**B**). Sites with more neurons have marginally, but significantly, more synapses (**C**), which is consistent with a lack of correlation between local synaptic density and the number of synapses per neuron (**D**), although a correlation between average number of synapses per neuron and local neuronal density, due to one outlier, cannot be discarded (**E**). Still, there is very clearly no correlation between local numbers of synapses per neuron and the ratio of endothelial cells per neuron (**F**); rather, the latter is directly, and strongly (r^2=0.750), correlated with the ratio of endothelial cells per synapse (or its inverse, the number of synapses per endothelial cell; **G**). All correlation coefficients are available in Table 6.

Table 6. Spearman correlation coefficients and p-values for correlations across cerebral cortical sites. DE, local density of endothelial cells; DN, local neuronal density; DG, local density of glial cells; DS, local density of synapses; E/N, ratio of endothelial cells per neuron; E/G, ratio of endothelial cells per glial cell; E/S, ratio of endothelial cells per synapse; G/N, ratio of glial cells per neuron; S/N, ratio of synapses per neuron; S/G, ratio of synapses per glial cell. All values pertaining to DE, DN and DG were obtained in the present study, from analysis of 2D images acquired in locations matching those described in (*21*); all values pertaining do DS were calculated from (*21*).

	D_E	D_N	D_G	D_S	E/N	E/G	E/S	G/N	S/N	S/G
D_E		-0.084, 0.7047	0.412, 0.0509	-0.194, 0.4133	**0.753, <0.0001**	**0.741, <0.0001**	**0.906, <0.0001**	0.123, 0.5758	-0.166, 0.4837	-0.393, 0.0862
D_N	-0.084, 0.7047		0.307, 0.1542	*0.460, 0.0414*	**-0.652, 0.0007**	-0.121, 0.5820	-0.235, 0.3177	**-0.624, 0.0015**	**-0.545, 0.0129**	0.056, 0.8113
D_G	0.412, 0.0509	0.307, 0.1542		0.108, 0.6488	0.128, 0.5605	-0.203, 0.3525	0.312, 0.1803	*0.441, 0.0350*	-0.291, 0.2131	**-0.831, <0.0001**
D_S	-0.194, 0.4133	*0.460, 0.0414*	0.108, 0.6488		-0.441, 0.0517	-0.215, 0.3632	**-0.506, 0.0230**	-0.306, 0.1896	0.404, 0.0775	0.363, 0.1156
E/N	**0.753, <0.0001**	**-0.652, 0.0007**	0.128, 0.5605	-0.441, 0.0517		**0.630, 0.0013**	**0.750, 0.0001**	**0.516, 0.0118**	0.171, 0.4717	-0.306, 0.1893
E/G	**0.741, <0.0001**	-0.121, 0.5820	-0.203, 0.3525	-0.215, 0.3632	**0.630, 0.0013**		**0.628, 0.0030**	-0.273, 0.2069	0.435, 0.0555	0.252, 0.2838
E/S	**0.906, <0.0001**	-0.235, 0.3177	0.312, 0.1803	**-0.506, 0.0230**	**0.750, 0.0001**	**0.628, 0.0030**		0.250, 0.2868	-0.364, 0.1163	**-0.526, 0.0171**
G/N	0.123, 0.5758	**-0.624, 0.0015**	*0.441, 0.0350*	-0.306, 0.1896	**0.516, 0.0118**	-0.273, 0.2069	0.250, 0.2868		0.235, 0.3177	**-0.669, 0.0013**
S/N	-0.166, 0.4837	**-0.545, 0.0129**	-0.291, 0.2131	0.404, 0.0775	0.171, 0.4717	0.435, 0.0555	-0.364, 0.1163	0.235, 0.3177		0.435, 0.0555
S/G	-0.393, 0.0862	0.056, 0.8113	**-0.831, <0.0001**	0.363, 0.1156	-0.306, 0.1893	0.252, 0.2838	**-0.526, 0.0171**	**-0.669, 0.0013**	0.435, 0.0555	

These data thus indicate that higher E/S is associated with higher E/N, even though there are not more endothelial cells where there are more synapses (or more neurons; Fig. 9A, B), and there are also not more E/N where there are more S/N (Fig. 9F). Rather, higher E/S occurs with higher E/N (Fig. 9G) simply due to small variations in endothelial cell densities that are not correlated with variations in densities of neurons or synapses (Fig. 9A-B) in the presence of significant local variations in neuronal densities that are only somewhat correlated with smaller variations in densities of synapses (Fig. 7C). Principal component analysis supports this conclusion: three factors are required to account for the variance in all six variables, with capillary density loading only in the first factor (explaining 42.9% of variance; factor loading,

573 0.996, associated with E/N [0.816] and E/S [0.926]), neuronal density loading only in the second
574 factor (total variance explained, 78.8%; loading, -0.943, associated with E/N [0.557] and S/N
575 [0.976]), and synaptic density as the sole contributor to the third factor (explaining a total of
576 99.3% of variance; factor loading, 0.981).

577 Finally, while the glia/neuron ratio is locally higher in cortical sites where the endothelial
578 cell/neuron ratio is also higher (Spearman, p=0.0118), the number of endothelial cells per
579 synapse is not correlated with the local glia/neuron ratio (p=0.2868; Table 6). Thus, a higher
580 proportion of glial cells per neuron is not associated with a larger capillary supply per synapse.

581

582 **Discussion**

583

584 While neuroscientists often frame the energy *cost* of the brain in terms of high neuronal
585 *demand* for energy, we prefer to reframe metabolism simply as energy *use*, a term that implies
586 nothing about what defines it, whether supply or demand, and instead leaves these open to
587 investigation. The issue of energetic *use* by neurons can then be separated into the more tractable
588 questions of (a) whether there is evidence that larger neurons *demand* and thus are provided with
589 more energy, depending on their intrinsic biophysical properties (Attwell and Laughlin, 2001),
590 and (b) whether there is evidence that larger neurons are *supplied* with more energy than smaller
591 neurons, regardless of (a). Our finding that local capillary area fraction or density of capillary
592 cells does not accompany the enormous variation in neuronal densities across sites in the mouse
593 brain nor synaptic densities in the mouse cerebral cortex provides evidence against (a) and in
594 support of (b), against several intuitive, but so far untested, central tenets of neurophysiology and
595 functional brain imaging, namely: that neurons *demand* energy, and larger neurons *demand* more

596 energy than smaller neurons; that sites with more synapses use more energy; that because larger
597 neurons have more synapses, they demand more energy; and that the steady-state density of the
598 adult capillary bed reflects self-organized adjustments across brain sites according to variations
599 in local energy demand. Instead, we interpret our data to indicate that, due to the 100x larger
600 variation in neuronal densities than in capillary density throughout the mouse brain, larger
601 neurons *get access* to more energy simply because where neurons are larger, as indicated by
602 lower neuronal densities, fewer neurons compete for the capillary density-restricted blood
603 supply. Similarly, we propose that, given a small but significant variation in densities of
604 synapses with densities of neurons within the cerebral cortex, there is a restricted range of
605 numbers of synapses per neuron, and more endothelial cells providing energy both per neuron
606 and per synapse where neurons are larger (highlighted middle panel in Fig. 1). These findings
607 suggest the intriguing possibility that increasing neuronal sizes in evolution may have brought
608 neurons the advantage of not decreasing energy availability per cell, and possibly holding that
609 constant, as body size increases and total metabolic rate scales more slowly than body mass
610 (Herculano-Houzel, 2011), a possibility that we are now ready to address by extending the
611 present analysis to other species.

612 Within the cerebral cortex in particular, a previous detailed study of variation in fractional
613 volume of the microvasculature across layers found that it varies little, and does not reflect
614 variations in neuronal density across cortical layers (Tsai et al., 2009). When compiling data
615 across layers, that study did find a significant positive correlation between neuronal density and
616 microvasculature volume fraction across sites, which our analysis corroborates when restricted to
617 the cerebral cortical gray matter alone (Table 5). Importantly, while this variation of capillary
618 density with neuronal density is significant across cortical sites, it is by no means large enough to

619 maintain a constant E/N ratio across cerebral cortical sites within the mouse brain: even within
620 the cerebral cortical gray matter, the E/N ratio still decreases with increasing neuronal density
621 (Table 5), which is indicative of less energy availability per neuron in these sites. Therefore, it
622 remains true for the cerebral cortex alone that our data suggest that energy availability per
623 neuron is supply-limited.

624 There are presently no direct data available on rates of energy use per neuron, whether in
625 different structures or species, to test the hypothesis that larger neurons use more energy
626 (whether due to supply or demand); all measurements so far have been of energy use per gram of
627 tissue (Mink et al., 1981; Karbowski, 2007), not per neuron. A necessary first step to establishing
628 whether larger neurons *use* more energy, be it due to increased demand, supply, or both, is
629 comparing average energy use per neuron where neurons have different sizes, both within and
630 across species. The practical impediment here is that measuring energy use requires bringing live
631 animals to the lab. We propose that local capillary density, which correlates very well, and
632 linearly, with resting blood flow and local rate of glucose use in both rat (Klein et al., 1986;
633 Borowsky and Collins, 1989) and macaque brains (Noda et al., 2002), and can be measured
634 readily and efficiently in 2D images of thin sections of fixed brains, is a good proxy and viable
635 alternative to estimating energy availability per volume as well as per neuron in fixed brain
636 tissue. While direct validation of the correspondence between local capillary density and resting
637 metabolic rate is underway, we expect that systematic analyses of local capillary densities will
638 provide a powerful tool to circumvent the limitations to studying energy use per neuron in living
639 animals. Indeed, we find that the small variations in the local vascular fraction measured as in the
640 present study across sites in the rat brain are a very good approximation of measurements of
641 local energy cost at rest in each structure (Ventura-Antunes, Dasgupta and Herculano-Houzel, in

642 preparation). These findings open the way to comparative studies of energy availability per
643 neuron in brains of species that are unlikely to ever be brought alive to laboratory settings.

644 While we examine fixed tissue and can make no claims about physiological properties and
645 dynamic changes in neurovascular coupling (Leithner and Royl, 2014), the fairly stable
646 distribution of the capillary bed in the perfused tissue compared to neuronal densities does
647 inform that there is more energy available per neuron in those sites with lower neuronal densities
648 (with few and larger neurons; Mota and Herculano-Houzel, 2014) than in sites of high neuronal
649 density. These findings are compatible with a scenario where neurons compete for a limited
650 energy supply, rather than the usually presumed scenario in which larger neurons and/or neurons
651 with more synapses *demand* more energy which is then provided as the capillary bed adapts to
652 those demands during development. A limited energy supply constrained by the density of the
653 capillary bed would have direct consequences for the level of neuronal and synaptic activity that
654 can be sustained across brain sites, in line with our previous suggestion that fundamental aspects
655 of neuronal structure and function are constrained by energy supply across species (Herculano-
656 Houzel, 2011). It remains to be determined whether these constraints manifest themselves during
657 development, for instance through the self-regulation of the numbers of synapses that can form
658 and remain active, or simply through self-regulation of levels of activity (as in synaptic
659 homeostasis; Turrigiano, 2012).

660 The present findings have fundamental implications for brain health and normal and diseased
661 aging. First, they suggest that the heightened vulnerability of the human white matter to ischemia
662 (Wang et al., 2016) may be primarily due to its low capillary density compared to gray matter
663 structures, and not simply to its large relative volume. Second, as cortical locations with high
664 neuron densities have far less blood supplied per neuron than locations with low neuronal

665 densities, individual neurons in "crowded" cortical areas are likely to be much more vulnerable
666 to aging and pathologies that compromise circulation and/or metabolic capacity. Most
667 remarkably, the hippocampus, whose granular layer contains most of its neurons and exhibits
668 some of the lowest values of E/N found here, is one of the brain structures most highly
669 vulnerable to hypoxia (Hossmann, 1999). Finally, some of the regions first and most vulnerable
670 to Alzheimer's disease are cortical areas with high resting metabolism (Buckner et al., 2005).
671 While that might be indicative of higher capillary densities that would increase energy
672 availability as a whole, it is possible that this is offset by very high neuronal densities, such as
673 those found in the entorhinal cortex and hippocampus here, leading to low values of E/N. We are
674 currently investigating the possibility that local variation in E/N correlates with brain tissue
675 vulnerability in normal and diseased aging.
676
677
678 **References**

679 Alle H, Roth A, Geiger JR. (2009) Energy-efficient action potentials in hippocampal mossy
680 fibers. Science 325, 1405-1408.
681
682 Ames III A (2000) CNS energy metabolism as related to function. Brain Res Rev 34, 42-68.
683
684 Aschoff J, Günther B, Kramer K (1971) Energiehaushalt und Temperaturregulation. Urban and
685 Schwarzenberg, Munich.
686

687 Attwell D, Laughlin SB (2001) An energy budget for signaling in the grey matter of the brain. J
688 Cereb Blood Flow Metab 21: 1133–1145.
689
690 Banavar JR, Damuth J, Maritan A, Rinaldo A (2002) Supply-demand balance and metabolic
691 scaling. Proc Natl Acad Sci 99, 10506-10509.
692
693 Boero JA, Ascher J, Arregui A, Rovainen C, Woolsey TA (1999) Increased brain capillaries in
694 chronic hypoxia. J Appl Physiol 86, 1211-1219.
695
696 Borowsky IW, Collins RC (1989) Metabolic anatomy of brain: a comparison of regional
697 capillary density, glucose metabolism, and enzyme activities. Journal of Comparative Neurology
698 288, 401-413.
699
700 Braitenberg V, Schüz A (1998) Cortex: Statistics and geometry of neuronal connectivity. Berlin:
701 Springer.
702
703 Buckner RL, Snyder AZ, Shannon BJ, LaRossa G, Sachs R, Fotenos AF, Sheline YI, Klunk WE,
704 Mathis CA, Morris JC, Mintun MA (2005) Molecular, structural, and functional characterization
705 of Alzheimer's disease: Evidence for a relationship between default activity, amyloid, and
706 memory. Journal of Neuroscience 25, 7709-7717.
707
708 Franklin K, Paxinos G (1997) The mouse brain in stereotaxic coordinates. New York, Elsevier.
709

710 Gundersen HJ, Jensen EB, Kieu K, Nielsen J (1999) The efficiency of systematic sampling in
711 stereology – reconsidered. J Microsc 193, 199-211.
712
713 Hainsworth FR, Collins BG, Wolf LL (1977) The function of torpor in hummingbirds. Physiol
714 Biochem Zool 50, 215-222.
715
716 Harris JJ, Jolivet R, Attwell D (2012) Synaptic energy use and supply. Neuron 75, 762-777.
717
718 Herculano-Houzel S (2011) Scaling of brain metabolism with a fixed energy budget per neuron:
719 implications for neuronal activity, plasticity and evolution. PloS One 6, e17514.
720
721 Herculano-Houzel S, Manger PR, Kaas JH (2014) Brain scaling in mammalian evolution as a
722 consequence of concerted and mosaic changes in numbers of neurons and average neuronal cell
723 size. Front Neuroanat 8, 77.
724
725 Herculano-Houzel S, Watson C, Paxinos G (2013) Distribution of neurons in functional areas of
726 the mouse cerebral cortex reveals quantitatively different cortical zones. Front Neuroanat 7, 35.
727
728 Hossmann KA (1999) The hypoxic brain. Insights from ischemia research. Adv Exp Med Biol
729 474, 155-169.
730
731 Howarth C, Peppiatt-Wildman CM, Attwell D (2010) The energy use associated with neural
732 computation in the cerebellum. J Cereb Blood Flow Metab 30, 403-414.
733

734 Hudetz AG (1997) Blood flow in the cerebral capillary network: a review emphasizing
735 observations with intravital microscopy. Microcirculation 4, 233-252.
736
737 Jie Z, An H, Coggan AR, Zhang X, Adil B, Muccigrosso D, Peterson LR, Gropler RJ (2014)
738 Non-contrast skeletal muscle oximetry. Magn Reson Med 71, doi:10.1002/mrm.24669.
739
740 Karbowski J (2007) Global and regional brain metabolic scaling and its functional consequences.
741 BMC Biol 5, 18.
742
743 Klein B, Kuschinsky W, Schrock H, Vetterlein F (1986). Interdependency of local capillary
744 density, blood flow, and metabolism in rat brains. American Journal of Physiology-Heart and
745 Circulatory Physiology 25, H1333-H1340.
746
747 Kuschinsky W, Paulson OB (1992) Capillary circulation in the brain. Cerebrovascular and Brain
748 Metabolism Reviews 4, 261-286.
749
750 Lauwers F, Cassot F, Lauwers-Cances V, Puwanarajah P, Duvernoy H (2008) Morphometry of
751 the human cerebral cortex microcirculation: general characteristics and space-related profiles.
752 Neuroimage 39, 936-948.
753
754 Leach RM, Treacher DF (1998) Oxygen transport – 2. Tissue hypoxia. BMJ 317, 1370-1373.
755
756 Leithner C, Royl G (2014) Oxygen paradox of neurovascular coupling. Journal of Cerebral
757 Blood Flow and Metabolism 34, 19-29.

758

759 Lin AL, Fox PT, Hardies J, Duong TQ, Gao JH (2010) Nonlinear coupling between cerebral
760 blood flow, oxygen consumption, and ATP production in human visual cortex. Proc Natl Acad
761 Sci USA 107, 8446-8451.

762

763 Madsen PL, Holm S, Herning M, Lassen NA (1993) Average blood flow and oxygen uptake in
764 the human brain during resting wakefulness: a critical appraisal of the Kety-Schmidt technique. J
765 Cereb Blood Flow Metab 13, 646-655.

766

767 Magistretti PJ (2006) Neuron-glia metabolic coupling and plasticity. J Exp Biol 209, 2304-2311.

768

769 Mink JW, Blumenschine RJ, Adams DB (1981) Ratio of central nervous system to body
770 metabolism in vertebrates: its constancy and functional basis. Am J Physiol Reg Integr Comp
771 Physiol 241, R203-R212.

772

773 Mota B, Herculano-Houzel S (2014) All brains are made of this: a fundamental building block of
774 brain matter with matching neuronal and glial masses. Front Neuroanat 8, 127.

775

776 Mullen RJ, Buck CR, Smith AM (1992) NeuN, a neuronal specific nuclear protein in vertebrates.
777 Development 116, 201-211.

778

779 Noda A, Ohba H, Kakiuchi T, et al. (2002) Age-related changes in cerebral blood flow and
780 glucose metabolism in conscious rhesus monkeys. Brain Research 936:76–81.

781

782 Pawlik G, Rackl A, Bing RJ (1981) Quantitative capillary topography and blood flow in the
783 cerebral cortex of cats: an in vivo microscopic study. Brain Res 208, 35-58.

784

785 Pellerin L, Magistretti PJ (2016) Neuroenergetics: calling upon astrocytes to satisfy hungry
786 neurons. The Neuroscientist 10, 53-62.

787

788 Ribeiro PFM, Ventura-Antunes L, Gabi M, Mota B, Grinberg LT, Farfel JM, Ferretti-Rebustini
789 REL, Leite REP, Filho WJ, Herculano-Houzel S (2013) The human cerebral cortex is neither one
790 nor many: neuronal distribution reveals two quantitatively different zones in the gray matter,
791 three in the white matter, and explains local variations in cortical folding. Front Neuroanat 7, 28.

792

793 Rolfe DFS, Brown GC (1997) Cellular energy utilization and molecular origin of standard
794 metabolic rate in mammals. Physiol Rev 77, 731-758.

795

796 Schölvinck ML, Howarth C, Attwell D (2008) The cortical energy needed for conscious
797 perception. Neuroimage 40, 1460-1468.

798

799 Schüz, A., & Palm, G. (1989). Density of neurons and synapses in the cerebral cortex of the
800 mouse. Journal of Comparative Neurology, 286(4), 442-455.

801

802 Tsai PS, Kaufhold JP, Blinder P, Friedman B, Drew PJ, Karten HJ, ... Kleinfeld D (2009)
803 Correlations of neuronal and microvascular densities in murine cortex revealed by direct
804 counting and colocalization of nuclei and vessels. J Neurosci 29, 14553-14570.
805
806 Turrigiano G (2012) Homeostatic synaptic plasticity: local and global mechanisms for stabilizing
807 neuronal function. Cold Spring Harbor Perspectives in Biology 4, a005736.
808 Wang Y, Liu G, Hong D, Chen F, Ji X, Cao G (2016) White matter injury in ischemic stroke.
809 Prog Neurobiol 141, 45-60.
810
811 Zhu F, Cizeron M, Qiu Z, Benavides-Piccione R, Kopanitsa MV, Skene NG, Koniaris B,
812 Defelipe J, Fransé E, Komiyama NH, Grant SGN (2018) Architecture of the mouse brain
813 synaptome. Neuron 99, 781-799.
814
815
816
817 **Table 5. Correlation analysis between variables across sites and animals.**
818

Dependent variable	Independent variable	Structure	N sites	Spearman rho	p-value	exponent	r^2	p-value
Figure 4A								
Endothelial cells/mm^3	**Capillary fraction, %**	**all**	**654**	**0.3450**	**<0.0001**	**0.460±0.046**	**0.135**	**<0.0001**
		Cx GM	**72**	**0.3151**	**0.0070**	**0.394±0.137**	**0.106**	**0.0052**
		Cx WM	**102**	**0.4118**	**<0.0001**	**0.479±0.124**	**0.130**	**0.0002**
		Hp MolL	55	-0.0015	0.9899	-0.009±0.122	0.000	0.9418
		Hp GranL	9	0.1487	0.3473	0.128±0.175	0.072	0.4864
		Hypothalamus	**79**	**0.6101**	**<0.0001**	**0.790±0.134**	**0.311**	**<0.0001**
		Thalamus	**121**	**0.5205**	**<0.0001**	**0.652±0.097**	**0.276**	**<0.0001**
		Striatum	**102**	**0.3561**	**0.0002**	**0.576±0.126**	**0.172**	**<0.0001**
		Cb MolL	43	-0.0127	0.9205	0.237±0.183	0.039	0.2015
		Cb GranL	46	0.2976	0.0209	0.086±0.233	0.003	0.7133
		Cb WM	25	-0.0100	0.9404	-0.037±0.185	0.002	0.8421

Endothelial cells/mm^2	**Capillary fraction, %**	**all**	**727**	**0.5942**	**<0.0001**	**0.676±0.034**	**0.350**	**<0.0001**
		Cx GM	**166**	**0.5882**	**<0.0001**	**0.771±0.068**	**0.439**	**<0.0001**
		Cx WM	**100**	**0.6407**	**<0.0001**	**0.728±0.104**	**0.333**	**<0.0001**
		Hp MolL	**28**	**0.5348**	**0.0034**	**0.340±0.125**	**0.223**	**0.0112**
		Hp GranL	**27**	**0.5107**	**0.0028**	**0.564±0.161**	**0.330**	**0.0017**
		Hypothalamus	**31**	**0.6072**	**0.0003**	**0.770±0.195**	**0.349**	**0.0005**
		Thalamus	**50**	**0.8044**	**<0.0001**	**0.961±0.093**	**0.691**	**<0.0001**
		Striatum	**62**	**0.5044**	**<0.0001**	**0.637±0.126**	**0.300**	**<0.0001**
		Cb MolL	**97**	**0.5717**	**<0.0001**	**0.624±0.103**	**0.279**	**<0.0001**
		Cb GranL	**99**	**0.2863**	**0.0035**	**0.288±0.121**	**0.055**	**0.0197**
		Cb WM	**67**	**0.7388**	**<0.0001**	**0.825±0.086**	**0.585**	**<0.0001**
Figure 4B								
Neurons/mm^3	**Capillary fraction, %**	all	607	0.2726	<0.0001	0.155±0.080	0.006	0.0552
		Cx GM	72	0.3041	0.0094	0.292±0.130	0.067	0.0280
		Cx WM	47	0.3068	0.0008	0.368±0.309	0.030	0.2406
		Hp MolL	24	-0.0142	0.9035	0.184±0.170	0.050	0.2907
		Hp GranL	42	0.0494	0.6694	0.241±0.172	0.076	0.1734
		Hypothalamus	**79**	**0.2989**	**0.0075**	**0.383±0.126**	**0.107**	**0.0032**
		Thalamus	**122**	**0.1946**	**0.0318**	**0.351±0.108**	**0.081**	**0.0015**
		Striatum	102	0.2350	0.0174	0.221±0.087	0.060	0.0127
		Cb MolL	57	0.0954	0.4535	0.335±0.232	0.036	0.1544
		Cb GranL	60	-0.1562	0.2334	-0.102±0.110	0.015	0.3537
		Cb WM	25	-0.1637	0.2194	n.a.		
Neurons/mm^2	**Capillary fraction, %**	**all**	**628**	**0.2579**	**<0.0001**	**0.464±0.115**	**0.026**	**<0.0001**
		Cx GM	**166**	**0.3119**	**<0.0001**	**0.337±0.068**	**0.128**	**<0.0001**
		Cx WM	47	-0.0467	0.6408	0.529±0.356	0.047	0.1436
		Hp MolL	21	-0.0883	0.6552	-0.328±0.316	0.053	0.3128
		Hp GranL	31	-0.0761	0.6790	-0.065±0.104	0.013	0.5396
		Hypothalamus	31	-0.0434	0.8169	0.125±0.184	0.016	0.5038
		Thalamus	50	0.3228	0.0222	0.342±0.143	0.107	0.0206
		Striatum	62	0.3504	0.0052	0.446±0.143	0.139	0.0028
		Cb MolL	97	0.0835	0.4159	0.059±0.119	0.002	0.6223
		Cb GranL	**102**	**-0.3804**	**<0.0001**	**-0.242±0.084**	**0.077**	**0.0047**
		Cb WM	97	0.0835	0.4159	0.059±0.119	0.002	0.6223
Figure 5A								
Glia/mm^3	**Neurons/mm^3**	**all**	**528**	**-0.3976**	**<0.0001**	**-0.162±0.024**	**0.080**	**<0.0001**
		Cx GM	72	0.2398	0.0425	0.162±0.107	0.031	0.1368
		Cx WM	47	-0.2684	0.0034	-0.154±0.080	0.077	0.0588
		Hp MolL	22	-0.0575	0.6241	0.252±0.291	0.036	0.3953
		Hp GranL	16	-0.3542	0.0214	0.084±0.519	0.002	0.8729
		Hypothalamus	78	0.1997	0.0776	0.259±0.122	0.056	0.0378
		Thalamus	122	0.1891	0.0370	0.143±0.090	0.021	0.1141
		Striatum	102	0.0844	0.3989	0.050±0.107	0.002	0.6376
		Cb MolL	35	-0.4620	0.0001	0.096±0.154	0.096	0.0705

		Cb GranL	32	0.3707	0.0035	0.959±0.377	0.178	0.0163
		Cb WM	35	-0.4620	0.0001	-0.287±0.154	0.096	0.0705
Glia/mm^2	**Neurons/mm^2**	**all**	**619**	**-0.5202**	**<0.0001**	**-0.257±0.020**	**0.212**	**<0.0001**
		Cx GM	**166**	**0.6817**	**<0.0001**	**0.888±0.072**	**0.485**	**<0.0001**
		Cx WM	47	0.2505	0.0111	0.029±0.029	0.022	0.3177
		Hp MolL	21	0.0899	0.6491	0.038±0.120	0.005	0.7529
		Hp GranL	24	-0.2723	0.1316	-0.153±0.332	0.010	0.6397
		Hypothalamus	31	-0.0637	0.7335	-0.097±0.186	0.009	0.6044
		Thalamus	50	-0.1676	0.2446	-0.156±0.122	0.033	0.2082
		Striatum	**62**	**0.4281**	**0.0005**	**0.447±0.108**	**0.222**	**0.0001**
		Cb MolL	97	-0.1563	0.1263	-0.222±0.162	0.020	0.1720
		Cb GranL	**100**	**0.3934**	**<0.0001**	**1.239±0.176**	**0.336**	**<0.0001**
		Cb WM	21	0.0064	0.9591	0.206±0.093	0.204	0.0399
Figure 5B								
Endothelial cells/mm^3	**Neurons/mm^3**	**all**	**530**	**0.1499**	**<0.0001**	**0.132±0.024**	**0.053**	**<0.0001**
		Cx GM	72	0.2430	0.0397	0.149±0.127	0.019	0.2442
		Cx WM	44	0.3494	0.0001	0.011±0.086	0.011	0.4984
		Hp MolL	15	-0.0910	0.4374	-0.132±0.244	0.022	0.5969
		Hp GranL	9	-0.1646	0.2975	-0.050±0.330	0.003	0.8849
		Hypothalamus	79	0.2225	0.0487	0.211±0.136	0.030	0.1239
		Thalamus	121	0.1084	0.2346	0.138±0.092	0.019	0.1343
		Striatum	**102**	**0.3594**	**0.0002**	**0.606±0.142**	**0.154**	**<0.0001**
		Cb MolL	40	0.1462	0.2489	0.302±0.101	0.190	0.0049
		Cb GranL	46	0.1482	0.2584	0.261±0.283	0.019	0.3616
		Cb WM	2	n.a.		n.a.		
Endothelial cells/mm^2	**Neurons/mm^2**	**all**	**620**	**0.1058**	**0.0041**	**0.035±0.016**	**0.008**	**0.0301**
		Cx GM	**166**	**0.6777**	**<0.0001**	**0.845±0.070**	**0.467**	**<0.0001**
		Cx WM	46	-0.0097	0.9226	0.378±0.061	0.465	<0.0001
		Hp MolL	21	0.0949	0.6311	0.003±0.114	0.000	0.9818
		Hp GranL	27	-0.4297	0.0141	-0.214±0.270	0.024	0.4372
		Hypothalamus	31	0.1024	0.5835	0.162±0.240	0.015	0.5058
		Thalamus	**50**	**0.3409**	**0.0154**	**0.492±0.142**	**0.199**	**0.0012**
		Striatum	**62**	**0.4886**	**<0.0001**	**0.399±0.115**	**0.168**	**0.0010**
		Cb MolL	97	0.0017	0.9865	-0.009±0.104	0.000	0.9281
		Cb GranL	**99**	**0.1937**	**0.0511**	**0.396±0.131**	**0.085**	**0.0033**
		Cb WM	21	-0.0364	0.7700	0.187±0.111	0.130	0.1076
Figure 5C								
Endothelial cells/mm^3	**Glia/mm^3**	**all**	609	0.0733	0.0394	-0.038±0.042	0.001	0.3719
		Cx GM	72	0.1622	0.1733	0.314±0.135	0.071	0.0233
		Cx WM	102	-0.0497	0.5943	-0.168±0.120	0.019	0.1626
		Hp MolL	49	0.1563	0.1804	0.041±0.103	0.003	0.6895
		Hp GranL	4	0.0782	0.6227	0.500±0.500	0.333	0.4226
		Hypothalamus	**78**	**0.4838**	**<0.0001**	**0.496±0.113**	**0.203**	**<0.0001**
		Thalamus	**121**	**0.2868**	**0.0014**	**0.342±0.087**	**0.114**	**0.0001**

		Striatum	102	0.1675	0.0924	0.232±0.142	0.026	0.1060
		Cb MolL	31	0.2535	0.0435	-0.032±0.128	0.002	0.8017
		Cb GranL	26	0.1674	0.2010	0.166±0.155	0.046	0.2946
		Cb WM	24	-0.0869	0.5165	0.129±0.130	0.043	0.3316
Endothelial cells/mm^2	**Glia/mm^2**	**all**	**719**	**0.2327**	**<0.0001**	**0.180±0.025**	**0.069**	**<0.0001**
		Cx GM	**166**	**0.6092**	**<0.0001**	**0.607±0.059**	**0.393**	**<0.0001**
		Cx WM	100	0.2706	0.0060	0.463±0.183	0.061	0.0132
		Hp MolL	28	0.0958	0.6278	0.189±0.189	0.037	0.3284
		Hp GranL	21	0.1771	0.3322	0.320±0.185	0.136	0.0995
		Hypothalamus	31	0.3218	0.0775	0.434±0.226	0.112	0.0651
		Thalamus	50	0.3048	0.0314	0.315±0.179	0.060	0.0858
		Striatum	**62**	**0.4523**	**0.0002**	**0.411±0.121**	**0.161**	**0.0012**
		Cb MolL	**97**	**0.4590**	**<0.0001**	**0.250±0.060**	**0.152**	**<0.0001**
		Cb GranL	**97**	**0.4635**	**<0.0001**	**0.343±0.055**	**0.292**	**<0.0001**
		Cb WM	67	0.2578	0.0352	0.293±0.138	0.065	0.0375
Figure 6A								
Glia/neuron	**Neurons/mm^3**	**all**	**528**	**-0.7611**	**<0.0001**	**-1.162±0.024**	**0.816**	**<0.0001**
		Cx GM	**72**	**-0.5422**	**<0.0001**	**-0.838±0.107**	**0.465**	**<0.0001**
		Cx WM	**47**	**-0.8862**	**<0.0001**	**-1.154±0.080**	**0.823**	**<0.0001**
		Hp MolL	22	-0.5863	0.0026	-0.747±0.291	0.248	0.0182
		Hp GranL	16	-0.4273	0.0048	-0.915±0.519	0.182	0.0996
		Hypothalamus	**78**	**-0.5376**	**<0.0001**	**-0.741±0.122**	**0.325**	**<0.0001**
		Thalamus	**122**	**-0.6216**	**<0.0001**	**-1.857±0.090**	**0.430**	**<0.0001**
		Striatum	**102**	**-0.5799**	**<0.0001**	**-0.949±0.107**	**0.440**	**<0.0001**
		Cb MolL	**35**	**-0.5250**	**<0.0001**	**-1.287±0.154**	**0.680**	**<0.0001**
		Cb GranL	32	0.2515	0.0525	-0.041±0.377	0.000	0.9146
		Cb WM	2	n.a.		n.a.		
		GM structures	**479**	**-0.7038**	**<0.0001**	**-1.087±0.032**	**0.708**	**<0.0001**
Glia/neuron	**Glia/mm^3**	**all**	**528**	**0.7820**	**<0.0001**	**1.495±0.073**	**0.444**	**<0.0001**
		Cx GM	**72**	**0.6163**	**<0.0001**	**0.806±0.129**	**0.359**	**<0.0001**
		Cx WM	**47**	**0.5395**	**<0.0001**	**1.499±0.257**	**0.430**	**<0.0001**
		Hp MolL	**22**	**0.8532**	**<0.0001**	**0.856±0.166**	**0.571**	**<0.0001**
		Hp GranL	**16**	**0.9882**	**<0.0001**	**0.978±0.137**	**0.783**	**<0.0001**
		Hypothalamus	**78**	**0.6404**	**<0.0001**	**0.786±0.101**	**0.441**	**<0.0001**
		Thalamus	**122**	**0.5863**	**<0.0001**	**0.856±0.090**	**0.427**	**<0.0001**
		Striatum	**102**	**0.7138**	**<0.0001**	**0.956±0.093**	**0.512**	**<0.0001**
		Cb MolL	**35**	**0.9471**	**<0.0001**	**1.333±0.178**	**0.629**	**<0.0001**
		Cb GranL	**32**	**0.9816**	**<0.0001**	**0.815±0.073**	**0.807**	**<0.0001**
		Cb WM	2	n.a.		n.a.		
		GM structures	**479**	**0.7670**	**<0.0001**	**1.177±0.065**	**0.410**	**<0.0001**
Glia/neuron	**Endothelial cells/mm^3**	**all**	**491**	**0.1041**	**0.0103**	**-0.247±0.095**	**0.014**	**0.0096**
		Cx GM	72	0.0362	0.7626	0.098±0.136	0.007	0.4757
		Cx WM	44	-0.1710	0.2505	0.075±0.350	0.001	0.8320
		Hp MolL	14	0.1413	0.5103	1.008±0.412	0.333	0.0307
		Hp GranL	4	0.1012	0.5238	0.938±0.479	0.658	0.1890

		Hypothalamus	78	0.1961	0.0832	0.265±0.119	0.061	0.0293
		Thalamus	121	0.1350	0.1381	0.199±0.117	0.024	0.0928
		Striatum	102	-0.1644	0.0987	-0.143±0.092	0.024	0.1225
		Cb MolL	28	0.2339	0.0799	-0.712±0.460	0.084	0.1339
		Cb GranL	26	0.1136	0.3873	0.44±0.246	0.001	0.8591
		Cb WM	2	n.a.		n.a.		
		GM structures	445	0.1706	<0.0001	-0.012±0.079	0.000	0.8834
Figure 6B								
Glia/neuron	**Neurons/mm^2**	**all**	**619**	**-0.8450**	**<0.0001**	**-1.257±0.020**	**0.865**	**<0.0001**
		Cx GM	166	-0.1281	0.1001	-0.111±0.072	0.014	0.1211
		Cx WM	**47**	**-0.9650**	**<0.0001**	**-0.971±0.029**	**0.962**	**<0.0001**
		Hp MolL	**21**	**-0.8285**	**<0.0001**	**-0.962±0.120**	**0.771**	**<0.0001**
		Hp GranL	**24**	**-0.5765**	**0.0006**	**-1.153±0.322**	**0.368**	**0.0017**
		Hypothalamus	**31**	**-0.6972**	**<0.0001**	**-1.097±0.186**	**0.545**	**<0.0001**
		Thalamus	**50**	**-0.7806**	**<0.0001**	**-1.156±0.122**	**0.651**	**<0.0001**
		Striatum	**62**	**-0.5830**	**<0.0001**	**-0.552±0.108**	**0.303**	**<0.0001**
		Cb MolL	**97**	**-0.5924**	**<0.0001**	**-1.222±0.162**	**0.376**	**<0.0001**
		Cb GranL	100	-0.0052	0.9587	0.239±0.176	0.018	0.1769
		Cb WM	**21**	**-0.8909**	**<0.0001**	**-0.794±0.093**	**0.792**	**<0.0001**
		GM structures	**551**	**-0.7925**	**<0.0001**	**-1.124±0.029**	**0.734**	**<0.0001**
Glia/neuron	**Glia/mm^2**	**all**	**619**	**0.7222**	**<0.0001**	**1.824±0.064**	**0.569**	**<0.0001**
		Cx GM	**166**	**0.5901**	**<0.0001**	**0.454±0.044**	**0.395**	**<0.0001**
		Cx WM	47	0.1093	0.4646	0.241±0.751	0.002	0.7493
		Hp MolL	21	0.3554	0.1138	0.861±0.436	0.170	0.0630
		Hp GranL	**24**	**0.9211**	**<0.0001**	**0.726±0.140**	**0.726**	**<0.0001**
		Hypothalamus	**31**	**0.6895**	**<0.0001**	**1.096±0.184**	**0.552**	**<0.0001**
		Thalamus	**50**	**0.7051**	**<0.0001**	**1.210±0.165**	**0.528**	**<0.0001**
		Striatum	**62**	**0.4399**	**0.0003**	**0.504±0.120**	**0.227**	**<0.0001**
		Cb MolL	**97**	**0.8495**	**<0.0001**	**1.088±0.064**	**0.754**	**<0.0001**
		Cb GranL	**100**	**0.8797**	**<0.0001**	**0.729±0.038**	**0.785**	**<0.0001**
		Cb WM	21	-0.0494	0.8318	0.010±0.449	0.000	0.9816
		GM structures	**551**	**0.6442**	**<0.0001**	**1.263±0.061**	**0.438**	**<0.0001**
Glia/neuron	**Endothelial cells/mm^2**	**all**	**612**	**0.1768**	**<0.0001**	0.302±0.134	0.008	0.0247
		Cx GM	166	0.0765	0.3273	0.094±0.058	0.016	0.1051
		Cx WM	**46**	**-0.1882**	**0.2052**	**-1.080±0.214**	**0.367**	**<0.0001**
		Hp MolL	21	0.0825	0.7221	0.231±0.503	0.011	0.6517
		Hp GranL	21	0.2869	0.1113	0.571±0.303	0.158	0.0748
		Hypothalamus	31	0.1565	0.4006	0.164±0.210	0.021	0.4405
		Thalamus	50	-0.0167	0.9086	-0.213±0.185	0.027	0.2545
		Striatum	62	-0.0528	0.6838	-0.029±0.133	0.001	0.8258
		Cb MolL	**97**	**0.3234**	**0.0012**	**0.620±0.191**	**0.100**	**0.0016**
		Cb GranL	**97**	**0.4672**	**<0.0001**	**0.641±0.114**	**0.250**	**<0.0001**
		Cb WM	21	-0.2117	0.3570	-0.426±0.383	0.061	0.2793
		GM structures	**545**	**0.3382**	**<0.0001**	**0.998±0.093**	**0.174**	**<0.0001**
Figure 7A								

Endothelial cells/neuron	**Neurons/mm^3**	**all**	**530**	**-0.6724**	**<0.0001**	**-0.868±0.024**	**0.706**	**<0.0001**
		Cx GM	**72**	**-0.4863**	**<0.0001**	**-0.851±0.127**	**0.390**	**<0.0001**
		Cx WM	**44**	**-0.6024**	**<0.0001**	**-1.058±0.086**	**0.784**	**<0.0001**
		Hp MolL	15	-0.0667	0.7567	**-1.132±0.244**	**0.624**	**0.0005**
		Hp GranL	9	-0.2148	0.1719	-1.050±0.330	0.591	0.0155
		Hypothalamus	**79**	**-0.5261**	**<0.0001**	**-0.788±0.136**	**0.304**	**<0.0001**
		Thalamus	**121**	**-0.6059**	**<0.0001**	**-0.862±0.092**	**0.426**	**<0.0001**
		Striatum	**102**	**-0.3124**	**0.0014**	**-0.394±0.142**	**0.072**	**0.0065**
		Cb MolL	**40**	**-0.4594**	**0.0003**	**-0.698±0.101**	**0.556**	**<0.0001**
		Cb GranL	46	-0.1465	0.2642	-0.739±0.283	0.134	0.0122
		Cb WM	2	n.a.		n.a.		
		GM structures	**484**	**-0.6379**	**<0.0001**	**-0.879±0.032**	**0.612**	**<0.0001**
Endothelial cells/neuron	**Glia/mm^3**	**all**	**491**	**0.4007**	**<0.0001**	**0.521±0.078**	**0.083**	**<0.0001**
		Cx GM	72	0.0621	0.6045	0.120±0.178	0.006	0.5007
		Cx WM	44	-0.0228	0.8794	0.371±0.327	0.030	0.2627
		Hp MolL	14	0.2353	0.2683	0.119±0.382	0.008	0.7601
		Hp GranL	4	0.0957	0.5464	0.244±0.898	0.036	0.8109
		Hypothalamus	78	0.2155	0.0565	0.282±0.146	0.047	0.0568
		Thalamus	121	0.0983	0.2815	0.197±0.120	0.022	0.1024
		Striatum	102	0.1512	0.1293	0.188±0.136	0.019	0.1710
		Cb MolL	28	0.4360	0.0007	0.354±0.194	0.114	0.0785
		Cb GranL	26	0.0595	0.6515	0.028±0.141	0.002	0.8419
		Cb WM	2	n.a.		n.a.		
		GM structures	**445**	**0.3614**	**<0.0001**	**0.304±0.075**	**0.036**	**<0.0001**
Endothelial cells/neuron	**Endothelial cells/mm^3**	**all**	**530**	**0.5915**	**<0.0001**	**0.600±0.074**	**0.112**	**<0.0001**
		Cx GM	**72**	**0.6810**	**<0.0001**	**0.870±0.110**	**0.471**	**<0.0001**
		Cx WM	**44**	**0.6229**	**<0.0001**	**1.188±0.274**	**0.308**	**<0.0001**
		Hp MolL	**15**	**0.9729**	**<0.0001**	**1.167±0.309**	**0.524**	**0.0023**
		Hp GranL	9	0.9942	<0.0001	1.065±0.431	0.466	0.0429
		Hypothalamus	**79**	**0.6696**	**<0.0001**	**0.856±0.093**	**0.526**	**<0.0001**
		Thalamus	**121**	**0.6790**	**<0.0001**	**0.864±0.090**	**0.437**	**<0.0001**
		Striatum	**102**	**0.7182**	**<0.0001**	**0.745±0.060**	**0.610**	**<0.0001**
		Cb MolL	40	0.7711	<0.0001	0.371±0.211	0.076	0.0860
		Cb GranL	**46**	**0.9230**	**<0.0001**	**0.927±0.079**	**0.759**	**<0.0001**
		Cb WM	2	n.a.		n.a.		
		GM structures	**484**	**0.6704**	**<0.0001**	**0.760±0.063**	**0.231**	**<0.0001**
Figure 7B								
Endothelial cells/neuron	**Neurons/mm^2**	**all**	**620**	**-0.8553**	**<0.0001**	**-0.965±0.016**	**0.853**	**<0.0002**
		Cx GM	166	-0.1877	0.0155	-0.155±0.070	0.029	0.0290
		Cx WM	**46**	**-0.8327**	**<0.0002**	**-0.621±0.061**	**0.701**	**<0.0001**
		Hp MolL	**21**	**-0.8893**	**<0.0001**	**-0.997±0.114**	**0.802**	**<0.0001**
		Hp GranL	**27**	**-0.7353**	**<0.0001**	**-1.214±0.270**	**0.446**	**0.0001**
		Hypothalamus	**31**	**-0.6492**	**<0.0001**	**-0.838±0.240**	**0.296**	**0.0016**
		Thalamus	**50**	**-0.5413**	**<0.0001**	**-0.508±0.142**	**0.209**	**0.0008**

		Striatum	**62**	**-0.5308**	**<0.0001**	**-0.601±0.115**	**0.314**	**<0.0001**
		Cb MolL	**97**	**-0.6847**	**<0.0001**	**-1.009±0.104**	**0.496**	**<0.0001**
		Cb GranL	**99**	**-0.4014**	**<0.0001**	**-0.604±0.131**	**0.179**	**<0.0001**
		Cb WM	**21**	**-0.8388**	**<0.0001**	**-0.813±0.111**	**0.739**	**<0.0001**
		GM structures	**553**	**-0.8243**	**<0.0001**	**-1.082±0.022**	**0.805**	**<0.0001**
Endothelial cells/neuron	**Glia/mm^2**	**all**	**612**	**0.5240**	**<0.0001**	**1.072±0.062**	**0.332**	**<0.0001**
		Cx GM	166	0.0492	0.5291	0.062±0.056	0.007	0.2722
		Cx WM	46	0.1352	0.3647	0.420±0.572	0.012	0.4666
		Hp MolL	21	-0.0007	0.9978	0.077±0.486	0.001	0.8765
		Hp GranL	21	0.2199	0.2266	0.423±0.245	0.136	0.1000
		Hypothalamus	31	0.3673	0.0421	0.530±0.266	0.120	0.0562
		Thalamus	50	0.3911	0.0050	0.525±0.170	0.166	0.0034
		Striatum	62	-0.0672	0.6037	-0.085±0.145	0.006	0.5618
		Cb MolL	**97**	**0.4094**	**<0.0001**	**0.337±0.086**	**0.140**	**0.0002**
		Cb GranL	97	0.1279	0.2001	0.066±0.069	0.010	0.3385
		Cb WM	21	-0.3355	0.1371	-0.640±0.452	0.095	0.1730
		GM structures	**545**	**0.3867**	**<0.0001**	**0.683±0.069**	**0.153**	**<0.0001**
Endothelial cells/neuron	**Endothelial cells/mm^2**	**all**	**620**	**0.3497**	**<0.0001**	**0.783±0.100**	**0.091**	**<0.0001**
		Cx GM	**166**	**0.5384**	**<0.0001**	**0.447±0.046**	**0.364**	**<0.0001**
		Cx WM	46	0.1956	0.1875	-0.230±0.199	0.029	0.2541
		Hp MolL	21	0.3531	0.1164	0.989±0.462	0.194	0.0455
		Hp GranL	**27**	**0.9011**	**<0.0001**	**1.114±0.144**	**0.704**	**<0.0001**
		Hypothalamus	**31**	**0.6278**	**0.0002**	**0.905±0.141**	**0.585**	**<0.0001**
		Thalamus	**50**	**0.5568**	**<0.0001**	**0.595±0.117**	**0.350**	**<0.0001**
		Striatum	**62**	**0.4069**	**0.0010**	**0.580±0.121**	**0.277**	**<0.0001**
		Cb MolL	**97**	**0.6868**	**<0.0001**	**1.009±0.101**	**0.513**	**<0.0001**
		Cb GranL	**99**	**0.7647**	**<0.0001**	**0.784±0.072**	**0.552**	**<0.0001**
		Cb WM	21	0.1443	0.5325	0.303±0.413	0.027	0.4726
		GM structures	**553**	**0.5258**	**<0.0001**	**1.283±0.078**	**0.329**	**<0.0001**
Figure 8								
Endothelial cells/neuron	**Glia/neuron (3D)**	**all**	**491**	**0.6371**	**<0.0001**	**0.645±0.023**	**0.609**	**<0.0001**
		Cx GM	**72**	**0.4862**	**<0.0001**	**0.629±0.109**	**0.323**	**<0.0001**
		Cx WM	**44**	**0.4673**	**0.0009**	**0.729±0.092**	**0.599**	**<0.0001**
		Hp MolL	**14**	**0.2512**	**0.2363**	**0.785±0.215**	**0.526**	**0.0033**
		Hp GranL	4	0.1230	0.4379	0.959±0.610	0.552	0.2567
		Hypothalamus	**78**	**0.5360**	**<0.0001**	**0.668±0.100**	**0.369**	**<0.0001**
		Thalamus	**121**	**0.5480**	**<0.0001**	**0.620±0.073**	**0.376**	**<0.0001**
		Striatum	**102**	**0.2816**	**0.0041**	**0.298±0.098**	**0.084**	**0.0032**
		Cb MolL	**28**	**0.4601**	**0.0003**	**0.424±0.084**	**0.493**	**<0.0001**
		Cb GranL	26	0.0474	0.7190	0.050±0.150	0.004	0.7425
		Cb WM	2	n.a.		n.a.		
		GM structures	**445**	**0.5986**	**<0.0001**	**0.635±0.031**	**0.482**	**<0.0001**
Endothelial cells/neuron	**Glia/neuron (2D)**	**all**	**612**	**0.8538**	**<0.0001**	**0.714±0.012**	**0.849**	**<0.0001**

		Cx GM	**166**	**0.2679**	**0.0005**	**0.300±0.074**	**0.091**	**<0.0001**
		Cx WM	**46**	**0.8774**	**<0.0001**	**0.652±0.056**	**0.755**	**<0.0001**
		Hp MolL	**21**	**0.8419**	**<0.0001**	**0.850±0.128**	**0.697**	**<0.0001**
		Hp GranL	**21**	**0.4367**	**0.0124**	**0.566±0.166**	**0.378**	**0.0030**
		Hypothalamus	**31**	**0.7157**	**<0.0001**	**0.623±0.154**	**0.361**	**0.0004**
		Thalamus	**50**	**0.6504**	**<0.0001**	**0.437±0.092**	**0.318**	**<0.0001**
		Striatum	**62**	**0.4926**	**<0.0001**	**0.521±0.120**	**0.237**	**<0.0001**
		Cb MolL	**97**	**0.6260**	**<0.0001**	**0.469±0.056**	**0.425**	**<0.0001**
		Cb GranL	**97**	**0.3471**	**0.0004**	**0.303±0.079**	**0.134**	**0.0002**
		Cb WM	**21**	**0.8004**	**<0.0001**	**0.854±0.144**	**0.649**	**<0.0001**
		GM structures	**545**	**0.6115**	**<0.0001**	**0.823±0.018**	**0.789**	**<0.0001**
Figure 9								
Endothelial cells/glia	**Endothelial cells/mm^2**	**Cx GM**	**23**	**0.741**	**<0.0001**	**0.801±0.158**	**0.551**	**<0.0001**
Endothelial cells/glia	**Endothelial cells/neuron**	**Cx GM**	**23**	**0.630**	**0.0013**	**0.707±0.146**	**0.528**	**<0.0001**
Endothelial cells/glia	**Endothelial cells/synapse**	**Cx GM**	**23**	**0.628**	**0.0030**	**0.622±0.167**	**0.435**	**0.0016**
Endothelial cells/neuron	**Endothelial cells/mm^2**	**Cx GM**	**23**	**0.753**	**<0.0001**	**0.862±0.152**	**0.604**	**<0.0001**
Endothelial cells/neuron	**Endothelial cells/synapse**	**Cx GM**	**23**	**0.750**	**0.0001**	**0.807±0.121**	**0.712**	**<0.0001**
Endothelial cells/neuron	**Glia/neuron**	**Cx GM**	**23**	**0.5156**	**0.0118**	0.550±0.274	0.161	0.0577
Endothelial cells/synapse	**Endothelial cells/mm^2**	**Cx GM**	**23**	**0.906**	**<0.0001**	**1.117±0.109**	**0.854**	**<0.0001**
Endothelial cells/synapse	**Endothelial cells/neuron**	**Cx GM**	**23**	**0.750**	**<0.0001**	**0.882±0.132**	**0.712**	**<0.0001**
Endothelial cells/synapse	**Synapses/mm^2**	**Cx GM**	**23**	**-0.506**	**0.0230**	**-1.515±0.478**	**0.358**	**0.0053**
Glia/mm^2	**Synapses/glia**	**Cx GM**	**23**	**-0.831**	**<0.0001**	**-0.784±0.104**	**0.759**	**<0.0001**
Glia/neuron	**Endothelial cells/neuron**	**Cx GM**	**23**	**0.516**	**0.0118**	0.293±0.146	0.161	0.0577
Glia/neuron	**Glia/mm^2**	**Cx GM**	**23**	**0.441**	**0.0350**	**0.634±0.191**	**0.344**	**0.0032**
Glia/neuron	**Neurons/mm^2**	**Cx GM**	**23**	**-0.624**	**0.0015**	**-0.592±0.212**	**0.270**	**0.0110**
Glia/neuron	**Synapses/glia**	**Cx GM**	**23**	**-0.669**	**0.0013**	**-0.688±0.143**	**0.562**	**0.0001**
Neurons/mm^2	**Synapses/mm^2**	**Cx GM**	**23**	**0.460**	**0.0414**	0.654±0.317	0.191	0.0541
Neurons/mm^2	**Synapses/neuron**	**Cx GM**	**23**	**-0.545**	**0.0129**	**-0.820±0.164**	**0.581**	**<0.0001**
Synapses/glia	**Endothelial cells/synapse**	**Cx GM**	**23**	**-0.526**	**0.0171**	**-0.378±0.167**	**0.222**	**0.0361**
Synapses/glia	**Glia/mm^2**	**Cx GM**	**23**	**-0.831**	**<0.0001**	**-0.969±0.129**	**0.759**	**<0.0001**
Synapses/glia	**Glia/neuron**	**Cx GM**	**23**	**-0.669**	**0.0013**	**-0.816±0.170**	**0.562**	**0.0001**
Synapses/neuron	**Neurons/mm^2**	**Cx GM**	**23**	**-0.545**	**0.0129**	**-0.708±0.142**	**0.581**	**<0.0001**
Synapses/neuron	**Synapses/mm^2**	**Cx GM**	**23**	**0.750**	**0.0001**	0.346±0.317	0.062	0.2890

821